Revista Facultad de Ingeniería

Title: Immune sliding mode control for formation tracking and obstacle avoidance of uncertain wheeled mobile robots

Authors: Willy John Nakamura Goto [1] https://orcid.org/0009-0006-2143-8812, Douglas Wildgrube Bertol [2] https://orcid.org/0000-0002-6980-7422 and Nardênio Almeida Martins [1, 2, 3*] https://orcid.org/0000-0001-9718-7673

[1] Department of Informatics, Postgraduate Program in Computer Science, Universidade Estadual de Maringá, Av. Colombo 5790, 87020-900 Maringá, Brasil.

[2] Department of Electrical Engineering, Systems Automation and Robotics Group, Universidade do Estado de Santa Catarina , Av. Madre Benvenuta 2007, Florianópolis, Brasil.

[3] Department of Automation and Systems, Robotics Research Group, Universidade Estadual de Maringá, Av. Colombo 5790, 87020-900 Maringá, Brasil.

Corresponding Author: Nardênio Almeida Ma
E-mail: namartins@uem.br

DOI: **10.17533/udea.redin.20250882**

To appear in: *Revista Facultad de Ingeniería Universidad de Antioquia*

Received: October 22, 2024
Accepted: September 15, 2025
Available Online: September 15, 2025

Revista Facultad de Ingeniería

Immune Sliding Mode Control for Formation Tracking and Obstacle Avoidance of Uncertain Wheeled Mobile Robots

Control inmune por modo deslizante para seguimiento y evasión en robots móviles

Authors:

Willy John Nakamura Goto [1], Douglas Wildgrube Bertol [2], and Nardênio Almeida Martins [1,2,3]

[1]Department of Informatics, Postgraduate Program in Computer Science, State University of Maringá.
[2]Department of Electrical Engineering, Systems Automation and Robotics Group, Santa Catarina State University.
[3]Department of Automation and Systems, Robotics Research Group, Federal University of Santa Catarina.

KEYWORDS:
Mobile Robotics, Multi-robot Control Systems Design, Robust Automatic Control, Trajectory Tracking, Artificial Immune Systems.

Robótica Móvil, Diseño de Sistemas de Control Multirobot, Control Automático Robusto, Seguimiento de Trayectoria, Sistemas Inmunitarios Artificiales.

ABSTRACT: In this article, for nonholonomic wheeled mobile robots subject to disturbances and uncertainties, a kinematic controller based on sliding mode control, artificial immune systems, and fuzzy logic is proposed and integrated with a proportional and derivative dynamic controller. The trajectory tracking is addressed and extended through the separation-bearing composition to the leader-follower formation control. To deal with the drawbacks of a traditional sliding mode control, namely the chattering phenomenon and the requirement to know *a priori* the bounds of the effects of disturbances, inspired by a regulation mechanism of the humoral adaptive immunity, it is derived a fuzzy system to establish the control reaction effect for an artificial immune system design to adjust online the gains of the control robustness portion adaptively. Furthermore, an obstacle avoidance strategy based on a reactive approach is also proposed, with a variable avoidance radius also considered, to navigate the leader robot around static obstacles during trajectory tracking during execution time. Simulation results in Matlab/Simulink and Gazebo demonstrate the effective performance, and the Lyapunov theory proves the stability of the proposed control system.

RESUMEN: En este artículo, un controlador cinemático basado en control por modo deslizante, sistemas inmunitarios artificiales y lógica difusa, integrado con un controlador dinámico proporcional-derivativo, es propuesto para robots móviles con ruedas no holonómicos sujetos a perturbaciones e incertidumbres. El seguimiento de la trayectoria se aborda y se extiende al control de formación líder-seguidor mediante la composición separation-bearing. Para abordar los inconvenientes del control por modo deslizante tradicional, concretamente el fenómeno de chattering y la necesidad de conocer a priori los límites de los efectos de las perturbaciones, se incorpora un sistema difuso, inspirado en un mecanismo de regulación de inmunidad adaptativa humoral, para establecer el efecto de reacción de control para un diseño de sistema inmunitario artificial para ajustar de forma adaptativa y en tiempo de ejecución las ganancias de la porción de robustez del control. Además, se propone una estrategia de evitación de obstáculos basada en un enfoque reactivo, considerando un radio de evitación variable, para guiar el robot líder alrededor de obstáculos estáticos durante el seguimiento de la trayectoria en tiempo de ejecución. Los resultados de la simulación en Matlab/Simulink y Gazebo demuestran la efectividad del enfoque propuesto, y la teoría de Lyapunov prueba la estabilidad del sistema de control.

1. Introduction

Trajectory tracking is a well-known control problem in the study of mobile robotics, where the robot must track a reference path with a temporal restriction. Multi-robotic systems have also drawn researchers' attention due to various applications (e.g., payload transportation, search, rescue, surveillance, and inspection tasks). Recent examples of the utility of robotics have been notable in the medical area, reducing the infection rate as well as support for supervision, welfare treatments, and other remote medical aids [1–3]. Each robot must be headed and kept in a desired group format in the formation control task.

Another relevant problem in practical applications is related to stability and robustness, as robots are subject to the incidence of uncertainties (which can arise from changes in mass/load, rotational inertia, unknown dynamics, rolling friction, and non-structured disturbances) [4]. This, together with the inherent nonlinearity of the robots, adds a challenge when dealing with motion performance, making trajectory tracking that accounts for system dynamics a subject of increasing interest. [5].

Obstacle avoidance (OA) controller is another possible constituent of an overall control architecture for motion tasks [6]. However, most research has considered only trajectory tracking or OA [7].

Underactuated systems have more degrees of freedom than control variables, and achieving effective control has become a hot topic in mechanical engineering, as their control problems are both challenging and meaningful due to nontrivial coupling characteristics and the influence of unexpected nonlinearities. [8]. The differential-drive wheeled mobile robot (DWMR) is a representative underactuated, nonlinear, and nonholonomic system with movement restrictions, featured as a simple mechanical structure widely applied in control

experiments [9].

For the sake of simplicity and to mitigate the drawbacks associated with error propagation due to a small number of robots in formation, this article employs the separation-bearing method in a leader–follower structure. This approach reduces the trajectory tracking problem to the essentials for the leader robot, while the follower robots are required to track the leader [10, 11] at a specified separation distance and bearing angle.

The triangular or "V" formation shape of three nodes is adopted since it is often used in regular missions, as it provides a particular view of the surrounding situation and proper communication without glaring hampers between the robots of the group [12].

Different nonlinear trajectory tracking controllers can be found in scientific publications, for example, neural network-inspired schemes [13], backstepping-type controllers [14], and optimization-based methods [15]. The first-order sliding mode control is popular due to its robustness properties. Denoted as SMC, it is a nonlinear control technique supplied by switching logic, driving the system trajectories towards a manifold (which is generally a sliding surface) and forcing it to slide along it (ensuring the sliding mode occurrence) [16]. Besides the methodological progress, the employment of the SMC has shown promising results in various functional applications in robotics and multiple agent systems, such as [17].

The choice of the control gains of the traditional SMC is generally associated with the bounds of the disturbances to guarantee its robustness features [18]. These bounds are primarily unknown, modeled inaccurately, and not often previously evaluated, which leads to a conservativeness issue, where a high control gain is chosen to ensure the stability of the system and fast convergence, but unwanted significant chattering can arise, as well as actuator degradation and unnecessary energy waste [18, 19].

Some research proposes an artificial immune system (AIS) to address these shortcomings, as in [20–24]. This paper proposes an AIS based on a response mechanism of the humoral/adaptive immunity to regulate the magnitude of the control effort by replacing the fixed gain of the sliding mode portion of the conservative SMC. For this, a fuzzy inference system (FIS) is designed to compute online the effect of the immunological reaction established by a nonlinear function of the AIS.

Researchers usually address trajectory tracking control problems, assuming that a collision-free reference has been previously generated [25, 26]. It is important to note that, in the case of trajectory tracking, tracking errors are expected to be driven toward zero, so the position (posture) of the robots is expected to be approximately the same as the goal (which can be updated every instant of time). Most works address reactive OA in the context of autonomous robot navigation or motion planning problems, determining a reasonable collision-free path between an initial and a final point, such that the robot must reach the target destination [27–29]. In this way, the concepts of the OA scheme can be treated, for example, in the formulation or modification of the reference trajectory during tracking or even through the decomposition into subproblems to be solved by different controllers. Thus, few studies address trajectory tracking while also considering obstacle avoidance [6, 7, 30, 31]. A local or reactive method is a suitable option to prevent collisions in execution time (online) by just updating the action according to the data locally obtained from the workspace and making the safety of the DWMR's motion more relevant than the optimality in this case [32]. Settling admissible movements for nonholonomic systems is not a trivial task. Still, it is more challenging with obstacle avoidance, since it requires the consideration of the spatial restrictions (due to obstacles), the structural restrictions of the robot, as well as the movement constraints due to the nonholonomy, to guarantee (ensure) the movement, safety, flexibility, and reliability of the robots [6, 33]. Regarding obstacle avoidance and trajectory tracking by nonholonomic robots, [6, 7, 30, 31] are studies that can be cited, in which an artificial potential field approach and a blending vector method in a switching scheme are proposed for obstacle avoidance, respectively. However, in these works, the formation control, the disturbances and uncertainties occurrence, and experiments are not considered. Moreover, the leader robot's safety in the considered formation structure is fundamental, since if it collides with an obstacle without a fault tolerance mechanism, the entire formation is compromised. Therefore, in addition to the robustness aspects, establishing a strategy to avoid obstacles for the leader DWMR is also relevant. In this paper, an OA reactive approach for static obstacles is considered, capable of changing the reference route during execution time.

This article presents as its major contribution an immune fuzzy sliding mode control (IFSMC) design in Cartesian coordinates for the kinematics, using the AIS-inspired approach. The regulation mechanism of the humoral immune response, together with the signum function that constitutes the sliding mode control portion, circumvents the need to know in advance the bounds of the effects of disturbances, realizes relevant chattering attenuation, guarantees the maintenance of the principle of invariance (one of the main characteristic properties of SMC,

in addition to accuracy, robustness, easy tuning, and implementation), and consequently, ensures the robustness to matched uncertainties in solving problems of trajectory tracking and leader-follower formation control, as well as obstacle avoidance. It is worth highlighting that even without replacing the discontinuous function of the classical control and without applying an adaptation rule, just with the gains computed by the AIS-based approach, the proposed control was able to suppress chattering while maintaining robustness aspects.

The following developments are considered necessary and just as important to achieve this main contribution. They are:

- The use of the separation-bearing method within the leader-follower structure for the formation control by uncertain and disturbed DWMRs in trajectory tracking attainment.
- As an alternative to [10], in the modeling of the reference for the leader and followers DWMRs, to enable maneuvers considering the nonholonomic non-slipping constraint and issues mainly regarding each DWMR orientation when a curve movement is performed, an auxiliary reference angular velocity is determined from the inverse kinematics.
- The design of the AIS-inspired gain in replacement of the fixed gain of the conservative SMC robustness portion by using the humoral immune response mechanism principles for the conception of a FIS with the Mamdani model to determine the effect of the immunological reaction, whose behavior is settled by a nonlinear function that represents the immune reaction effect so that the control effort magnitude can be online regulated adaptively.
- A reactive OA strategy and a variable avoidance radius to prevent the leader DWMR from colliding with circular-shaped singly static obstacles distributed along the trajectory during tracking;
- The analysis of Lyapunov that proves the stability of the closed-loop control system.
- Simulations carried out in Matlab/Simulink (version R2024b), as well as in the Gazebo Classic simulator (version 11.14) integrated with Matlab/Simulink. Analyzing the results, the performances of the SMC and IFSMC controllers were evaluated.

2. Problem Formulation

2.1 DWMR's Dynamic and Kinematic Models

The PowerBot robot has a mechanical structure composed of four conventional wheels: two active conventional and two passive casters. The kinematic and dynamic posture models sufficiently portray the system and are broadly covered in related research [11, 34, 35]. The uncertain DWMR's posture model vector, Eq. (1), is as follows [11, 35]:

$$\begin{bmatrix}\dot{q}\\ \dot{v}\end{bmatrix} = \begin{bmatrix} J(q)v \\ -\overline{M}^{-1}(q)\left(\overline{H}v + \overline{\tau}_b\right)\end{bmatrix} + \begin{bmatrix} 0 \\ \overline{M}^{-1}(q)\overline{E}(q)\end{bmatrix}\tau\,, \tag{1}$$

where $q = [x\ y\ \theta]^T$, $v = [v_l\ \omega_a]^T$ and $\tau = [\tau_r\ \tau_l]^T$ are the posture, the velocity and the torque vector of the robot respectively, being τ_r the torque in right wheel and τ_l in left one, and other terms are in Eq. (2):

$$J(q) = \begin{bmatrix} cos(\theta) & -dsin(\theta) \\ sin(\theta) & dcos(\theta) \\ 0 & 1\end{bmatrix}\,,\ \overline{M} = \begin{bmatrix} m & 0 \\ 0 & -md^2 + I\end{bmatrix}\,,$$
$$\overline{H}(q,\dot{q}) = \begin{bmatrix} 0 & -dm\dot{\theta} \\ dm\dot{\theta} & 0\end{bmatrix}\,,\ \overline{E} = \begin{bmatrix} \frac{r}{2} & \frac{r}{2} \\ \frac{r}{2b} & -\frac{r}{2b}\end{bmatrix}\,, \tag{2}$$

where d is the distance between the robot's center of mass and the intersection point of the wheel axis and the symmetry axis; m is the mass of the robot; I is the rotational inertia; b is measured from symmetry axis to the center of an actuated wheel of the robot; r is the radius of the actuated wheels; $\overline{M}(q)$ defines a known smooth nominal function related to the inertia matrix; $\overline{H}(q,\dot{q})$ refers to the centripetal and Coriolis matrix; and $\overline{E}(q)$ determines an input transformation matrix. Also, $\overline{\tau}_b = \Delta\overline{M}(q)\dot{v} + \Delta\overline{H}(q,\dot{q})v + \overline{\tau}_d$ is a way to retract uncertainties caused by inexactitudes in determining physical parameters, unpredictable dynamics from actuator and sensor, and non-parametric disturbances [35].

Thus, Eq. (1), in its first and second lines, introduces the kinematic and dynamic posture models, respectively, underlining that they are considered for synthesizing the kinematic and dynamic control.

2.2 Formation Control

The separation-bearing method within the leader-follower structure for the formation control aims to obtain, for the follower robot j, a control velocity vector v_{c_j} to satisfy conditions of Eq. (3) [10]:

$$\lim_{t\to\infty}(L_{ij_d} - L_{ij}) = 0\,;\ \lim_{t\to\infty}(\Psi_{ij_d} - \Psi_{ij}) = 0 \tag{3}$$

where L_{ij_d} denotes the wanted separation distance and Ψ_{ij_d}, the wanted bearing angle, while L_{ij} and Ψ_{ij} are the measured values from the follower robot j to the leader robot i. In addition to fulfilling the conditions of Eq. (3), smooth velocity inputs vector v_{c_j} has to fulfill $lim_{t\to\infty}(q_{r_j} - q_j) = 0$. And the torque τ_j, Eq. (1), is generated to comply with $lim_{t\to\infty}(v_{c_j} - v_j) = 0$. With these objectives realized, all robots i and j warrant tracking the formation trajectory by the entire robot group [11].

3. Controller Project

3.1 Kinematic Controller - SMC

Derivation of the SMC and its properties is done directly from the state space representation of the system given by Eq. (4):

$$\dot{q}_e = A_0(q_e, t) + B_0(q_e, t)v_c(t) + d_b(q_e, t) \tag{4}$$

where $q_e = [x_e\ y_e\ \theta_e]^T$ is the states vector or posture error; $A_0(q_e, t)$ is the nominal parameters' vector and $B_0(q_e, t)$, the nominal parameters' matrix; $v_c(t)$ is the control signals vector; and $d_b(q_e, t) = B_0(q_e, t)\tilde{d}_0$ with $\tilde{d}_0$ being the disturbances and uncertainties vector. In addition, the definition of the sliding surfaces is presented in Eqs. (5) and (6):

$$\sigma = \Lambda^T q_e = 0 \tag{5}$$

$$\sigma^* = B_{0_\sigma}^T \sigma = 0 \tag{6}$$

being matrix $\Lambda^T = \frac{\partial \sigma}{\partial q_e} > 0$ and $B_{0_\sigma} = \frac{\partial \sigma}{\partial q_e} B_0$. Using Eqs. (4) and (5), one has [34, 36, 37]:

$$\dot{\sigma} = \frac{\partial \sigma}{\partial q_e}\dot{q}_e + \frac{\partial \sigma}{\partial t} = A_{0_\sigma} + B_{0_\sigma} v_c + d_\sigma + \frac{\partial \sigma}{\partial t}, \tag{7}$$

where $A_{0_\sigma} = \frac{\partial \sigma}{\partial q_e} A_0$, $\frac{\partial \sigma}{\partial t} = 0$ and $d_\sigma = \frac{\partial \sigma}{\partial q_e} d_b = B_{0_\sigma}\tilde{d}_0$. As a result, the following control law for the DWMRs is obtained and shown by Eq. (8):

$$v_c = \underbrace{-B_{0_\sigma}^{-1} A_{0_\sigma}}_{\text{cp1}} - \underbrace{G\, sign(\sigma^*)}_{\text{cp2}} - \underbrace{P\, \sigma^*}_{\text{cp3}}, \tag{8}$$

which can be composed of three control portions: equivalent control (cp1), sliding mode (cp2), and reaching mode (cp3) portions, where G and P are positive definite diagonal matrices.

To guarantee robustness to matched uncertainties, the proof of the closed-loop control system's stability is carried out by the theory of Lyapunov using a candidate function V as Eq. (9):

$$V = \frac{1}{2}\sigma^T\sigma > 0\,, \tag{9}$$

where $\dot{V}$ is obtained after mathematical manipulation using Eqs. (6), (7) and (8), as shown in Eq. (10):

$$\begin{aligned}
\dot{V} &= \sigma^T\dot{\sigma} = \sigma^T B_{0_\sigma} B_{0_\sigma}^{-1} A_{0_\sigma} + \sigma^T B_{0_\sigma}(v_c + \tilde{d}_0) \\
&= \left(B_{0_\sigma}^T\sigma\right)^T B_{0_\sigma}^{-1} A_{0_\sigma} + \left(B_{0_\sigma}^T\sigma\right)^T (v_c + \tilde{d}_0) \\
&= -{\sigma^*}^T G sign(\sigma^*) - {\sigma^*}^T P\sigma^* + {\sigma^*}^T\tilde{d}_0 \\
&\leq -{\sigma^*}^T P\sigma^* - \left(\lambda_{\min}\{G\} - \tilde{d}_{0_M}\right)\|\sigma^*\| \leq 0
\end{aligned} \tag{10}$$

where $sign(\sigma^*) = \frac{\|\sigma^*\|}{\sigma^*} = \frac{\sigma^*}{\|\sigma^*\|}$; the smallest singular value of the matrix G given by $\lambda_{\min}\{G\}$; and the upper bound of $\tilde{d}_0$ can be represented by $\tilde{d}_{0_M}$ since it is assumed that $\tilde{d}_{0_v}$ and $\tilde{d}_{0_\omega}$ are limited by constants, i.e. there is a norm-bound $\|\tilde{d}_0\| \leq \tilde{d}_{0_M}$ or bound values such that $|\tilde{d}_{0_v}| \leq \tilde{d}_{0_{M_v}}$ and $|\tilde{d}_{0_\omega}| \leq \tilde{d}_{0_{M_\omega}}$.

Further information about the SMC design and stability analysis can be consulted in [34, 36, 37].

However, a standard sliding mode control portion (cp2), Eq. (8), requires knowing the limits of the effects of disturbances to carry out appropriate compensation, which can also cause the undesirable phenomenon of chattering. The AIS theory, specifically the immune response mechanism, is used to overcome these inconveniences.

3.2 Immune Reaction Principles of AIS

The biological immune system (BIS) primarily recognizes and represses antigens, which can be harmful agents and which trigger an immunological response (a cooperative and systematized reaction by the cells responsible for it). Two major immunity types that act cooperatively to defend the organism can be cited [38]: as the first defensive action line, the innate immunity promptly reacts and eliminates any pathogen; and, specialized to combat invaders associated with a specific antigen, the acquired or adaptive immunity has, as its two main classes, the humoral immunity and the cell-mediated one. This paper proposes an AIS inspired by the reaction mechanism of adaptive humoral immunity. The B and T cells (leukocytes or white blood cells named lymphocytes) are the primary cells responsible for this type of immune response, in which B lymphocytes produces antibodies (Ab) helping the immune system fight a particular antigen (Ag), and an antigen-presenting cell (APC) activates the T lymphocytes, which can be helper T cells (T_h) or suppressor/regulatory T cells (T_s). The first one stimulates the production of antibodies by B cells through the secretion of interleukin IL^+, and the second one smooths the T_h and B cells' activity to avoid exaggerated immunological reactions by producing interleukin IL^- for the stabilization of the

immune response. An illustrative diagram of this immune reaction mechanism is presented in Fig. 1.

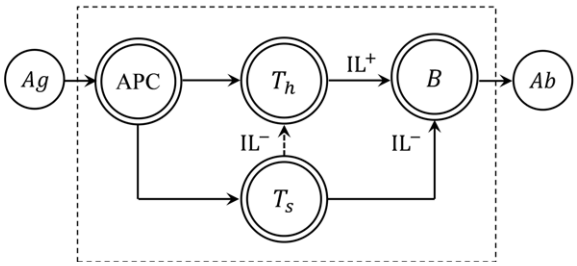

Figure 1 Simplified humoral immunity structure.

The AIS inspired by humoral immunity is usually designed to concentrate on the constraining effect on B lymphocytes. Thus, based on [39], the corresponding portions of the considered AIS structure can be derived by Eqs. (11), (12), and (13):

$$T_h = k_h(\varepsilon); \tag{11}$$
$$T_s = k_s(\varepsilon) f(\varepsilon, \Delta\varepsilon); \tag{12}$$

$$\begin{aligned} S_B &= T_h - T_s \\ &= k_h(\varepsilon) - k_s(\varepsilon) f(\varepsilon, \Delta\varepsilon) \\ &= k_h(\varepsilon)[1 - \eta f(\varepsilon, \Delta\varepsilon)] \end{aligned} \tag{13}$$

where a factor of proportionality $\eta = k_s(\varepsilon)/k_h(\varepsilon)$ describes the T lymphocyte interaction. Each term of the AIS and its meaning can be seen in [36], and a comparison between the adaptive control system and the immune regulation process is shown in [36, 37].
As can be seen in [21], [22] and [24], the enhancing factor k_h or the regulatory factor k_s can be adaptive parameters or variables in function of the amount of the antigen. The present article considers them as positive constants, as in [20] and [23].

3.3 Proposed kinematic controller inspired on AIS

The humoral immune mechanism can be introduced so that the sliding mode gains adaptive regulation, minimizing the control efforts and compensating for disturbances. In the AIS design, the sliding surface σ^* was considered to be the amount of the antigen, as in [20–24], and the gain G_{AIS} of the sliding mode portion of the proposed IFSMC, as the total stimulus sent to B lymphocytes for production of antibodies (Fig. 2).
Therefore, the resulting IFSMC control law, Eq. (14), can be established as follows:

$$v_c = -B_{0_\sigma}^{-1} A_{0_\sigma} - G_{AIS} sign(\sigma^*) - P\sigma^* \tag{14}$$

where, corresponding with Eq. (13), $G_{AIS} = k_h - k_s f$, and described by diagonal matrices.

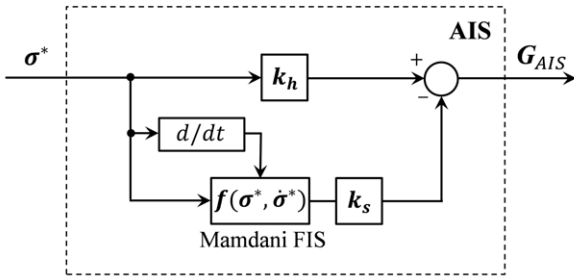

Figure 2 Proposed AIS control structure

In [21, 22, 24, 40], the nonlinear function that represents the immune response reaction, $f(\cdot)$, is obtained by an exponential relationship in function of the antigen amount. Whereas in [20, 23, 39–41], it is calculated by a FIS, generally taking into account the stimulatory signal for B cells and its variation, considering an immunological response with a delay. As it can also be seen from concepts in [36, 37] since the AIS regulatory effect can be determined by activating or restricting the activity of T_s cells, $f(\cdot)$ has its importance regarding the adjustment of the antibodies production by B cells. Regarding the control, the relevance lies in determining the suppression containment to enhance compensatory action against disturbances working to reduce errors or its stimulation to alleviate excessive efforts. In this article, to avoid time delays, the reaction effect is regulated by considering the antigen amount and its variation, as illustrated in Fig. 2, according to the principles described earlier in this section.
The function $f(\sigma^*, \dot{\sigma^*})$ is computed using a Mamdani-type FIS, chosen for its intuitiveness in interpretability, plausibility, and universal approximation property. Triangular membership functions (MFs) were adopted in the FIS design for its N inputs and M outputs. Besides that, fuzzification by singleton method, inference engine by-product, defuzzification by center average method, and K "if...then..." fuzzy rules, being the rule k as:

$$\begin{aligned} &\text{Rule } k\text{: IF } x_1 \text{ is } A_1^{(k)} \text{ and } \ldots \text{and } x_N \text{ is } A_N^{(k)} \\ &\qquad \text{THEN } y_1 \text{ is } B_1^{(k)} \text{ and } \ldots \text{and } y_M \text{ is } B_M^{(k)} \end{aligned}$$

being $x = (x_1, \ldots, x_n, \ldots, x_N)^T$ the input and $y = (y_1, \ldots, y_m, \ldots, y_M)^T$ the output of the fuzzy system, $A_n^{(k)}$ the fuzzy sets label in input space and $B_m^{(k)}$, in output space. The mth FIS crisp output, y_m, taking these considerations is calculated by Eq. (15) as [42]:

$$y_m = \frac{\sum_{k=1}^{K} c_m^{(k)} S_k}{\sum_{k=1}^{K} S_k} = C^T \xi(x)\,, \tag{15}$$

where $c_m^{(k)}$ is the mth output MF's center value in the

rule k, $\xi(x) = \left(\xi^{(1)}(x), \ldots, \xi^{(K)}(x)\right)^T$ is a regressive vector with $\xi^{(k)}(x) = S_k / \sum_{k=1}^{K} S_k$, and $S_k = \prod_{n=1}^{N} \mu_n^{(k)}(x_n)$ is the MFs' mappings product for all input variables in rule k, in which μ_n is the input MF. In this paper, the nonlinear function $f(\cdot)$ is the output of the fuzzy controller, whereas σ^* and $\dot{\sigma}^*$ are the input variables. By choosing triangular MFs, those related to input σ^* can be defined as in Eq. (16):

$$\mu_n^{(k)}(\sigma_n^*) = \begin{cases} 0; & \sigma_n^* \leq \alpha_1 \\ \dfrac{\sigma_n^* - \alpha_1}{\alpha_2 - \alpha_1}; & \alpha_1 \leq \sigma_n^* \leq \alpha_2 \\ \dfrac{\alpha_3 - \sigma_n^*}{\alpha_3 - \alpha_2}; & \alpha_2 \leq \sigma_n^* \leq \alpha_3 \\ 0; & \alpha_3 \leq \sigma_n^* \end{cases}, \quad (16)$$

where the triangle's base vertices are denoted by α_1 and α_3, and the peak, by α_2. The other input variable and the output MFs ($\mu_n(\dot{\sigma}_n^*)$ and $\mu_n(f_n)$) are calculated similarly. The procedures of the FIS used to compute the AIS function $f(\cdot)$, follow a structure similar to the flowchart presented in [43].

Based on the principles of the considered immune response, as in [36, 37] and briefly delineated in Section 3.2, the design of the set of fuzzy rules was established as presented in Table 1, where NB, NM, NS, ZO, PS, PM and PB denote Negative Big, Negative Middle, Negative Small, Zero, Positive Small, Positive Middle and Positive Big respectively. Seeing that negative and positive values can be obtained for the sliding variable σ^*, the assumption that there is a negative and a positive semi-cycle for the amount of the antigen can be taken into account. Unraveling, $\sigma^* > 0$ and $\dot{\sigma}^* < 0$, or $\sigma^* < 0$ and $\dot{\sigma}^* > 0$, can be a sign of antigen amount reduction; $\sigma^* > 0$ and $\dot{\sigma}^* > 0$, or $\sigma^* < 0$ and $\dot{\sigma}^* < 0$, can denote an antigens' consistency increasing. Values close to zero can be interpreted as the absence of detectable antigen levels and variations. Furthermore, the containment of the suppression reaction (enhancing the stimulus) is represented by $f \leq 0$, and the intensification of the inhibitory effect (to smooth effort), by $f > 0$.

Table 1 Set of fuzzy rules for the AIS function $f(\sigma^*, \dot{\sigma}^*)$.

			$\dot{\sigma}^*$		
σ^*	NB	NS	ZO	PS	PB
NB	NB	NM	NM	NS	NS
NS	NM	NS	ZO	PS	ZO
ZO	ZO	PS	PM	PS	ZO
PS	ZO	PS	ZO	NS	NM
PB	NS	NS	NM	NM	NB

A positive definite candidate Lyapunov function is chosen equivalently to Eq. (9) for the stability proof. To guarantee the sliding mode occurrence, using the sliding surface dynamics, Eq. (7), and Eq. (14) as the control law, $\dot{V} \leq 0$ is obtained as in Eq. (17):

$$\dot{V} \leq -{\sigma^*}^T P \sigma^* - \left(\lambda_{\min}\{G_{AIS}\} - \tilde{d}_{0_M}\right) \|\sigma^*\| . \quad (17)$$

An equivalent analysis on stability can be conducted by observing the similarity with Eq. (10). A bound is ensured for all $g_{n_{AIS}}$ (i.e. each gain of G_{AIS}) because k_{h_n} and k_{s_n} are positive constant parameters, and since it is obtained from Mamdani FIS, f_n is bounded with its discourse domain between a negative and a positive value ($-f_n^- \leq f_n \leq f_n^+$). It can be noted that when $k_{s_n} = 0$ or $f_n = 0$, the IFSMC is as a traditional SMC with $g_{n_{AIS}} = k_{h_n}$. And, to satisfy $g_{n_{AIS}} > 0$ (i.e. $k_{h_n} - k_{s_n} f_n > 0$), an upper bound for f_n can be such that $f_n < k_{h_n}/k_{s_n}$. Thus, this consideration can be taken into account in the design of the FIS to delimit a value for f_n^+. Given the above and remembering the zone of reaction determined by f_n, it can be seen that the restriction on the inhibitory action is pointed out by $k_{s_n} f_n < 0$, stimulating the gain $g_{n_{AIS}}$ increase, and its activation, by $0 < k_{s_n} f_n < k_{h_n}$, enabling a reduction on the gain $g_{n_{AIS}}$ to minimize the control efforts.

3.4 Dynamic Controller

For both the robots i (leader) and j (follower), the dynamic control aims to assure a rapid convergence of auxiliary velocity tracking errors ($v_e = v_c - v$) through the promoted torques applied to control the dynamic model of the DWMR with uncertainties and other non-linearities, Eq. (1). For the dynamic controller, as a proportional and derivative control (PD control), Eq. (18), with stability analysis proved by using Lyapunov theory, as in [11, 34, 35, 44], one considers:

$$\tau = \overline{E}(q)^{-1} \overline{u} , \quad (18)$$

where $\overline{u} = [\overline{u}_v \ \overline{u}_\omega]^T$ is a vector of control inputs taken into account by the dynamic control to obtain torques for a quick converging of v_c. In the domain of the frequency, it is determined by $C_v(s) = \frac{v(s)}{\overline{u}_v(s)} = (k_{p_v} + k_{d_v} N_v)/(1 + \frac{N_v}{s})$ and $C_\omega(s) = \frac{\omega(s)}{\overline{u}_\omega(s)} = k_{p_\omega} + (k_{d_\omega} N_\omega)/(1 + \frac{N_\omega}{s})$, where k_{p_v} and k_{p_ω} are the proportional gains, k_{d_v} and k_{d_ω} are the derivative gains, and N_v and N_ω are derivative filter parameter positive gains, which are set for a suitable performance in response time and stability achievement despite neglected dynamics, avoiding chattering [35].

3.5 Follower Control Design

Aiming to determine the necessary velocities ($v_{cj} = [v_{lcj} \ \omega_{acj}]^T$) for tracking of the leader robot i,

the kinematic controller of the follower robot j is designed considering a desired separation distance and bearing angle from the leader according to Eq. (3), which deals with formation control.
Describing the error dynamics, $\dot{q}_{ej}$, based on a nonlinear systems generic model similar to [11], and also adding a vector d_b to take into account effects of uncertainties (for example, external disturbances and modeling imprecision), the Eq. (19) is determined as:

$$\begin{aligned}\dot{q}_{ej} &= A_0(q_{ej},t) + B_0(q_{ej},t)v_{cj}(t) + d_b(q_j,t)\\ \begin{bmatrix}\dot{x}_{ej}\\ \dot{y}_{ej}\\ \dot{\theta}^*_{ej}\end{bmatrix} &= \begin{bmatrix}v_{li}cos(\theta_{ij}) - \omega_{ai}L_{ijd}sin(\Psi_{ijd}+\theta_{ij})\\ v_{li}sin(\theta_{ij}) - \omega_{ai}L_{ijd}cos(\Psi_{ijd}+\theta_{ij})\\ \omega^*_{ajr}\end{bmatrix} +\\ &+ \begin{bmatrix}-1 & y_{ej}\\ 0 & -(d_j+x_{ej})\\ 0 & -1\end{bmatrix}\begin{bmatrix}v_{lcj}+\tilde{d}_{0_v}\\ \omega_{acj}+\tilde{d}_{0_\omega}\end{bmatrix}, \end{aligned} \quad (19)$$

with $\theta_{ij} = \theta_i - \theta_j$, $d_b = B_0\tilde{d}_0$, v_{li} and ω_{ai} being the linear and angular velocities of the leader i respectively, and ω^*_{ajr} as auxiliary reference angular velocity derived from the inverse kinematics as in Eq. (20):

$$\omega^*_{ajr} = \frac{1}{d_j}\left(v_{li}sin(\theta^*_{\text{ijr}}) + L_{ijd}\omega_{ai}cos(\Psi_{ijd}+\theta^*_{\text{ijr}})\right) \quad (20)$$

where $\theta^*_{\text{ijr}} = \theta_i - \theta^*_{\text{jr}}$. Eq. (20) solves the problem in which each formation robot's orientation might not be alike, especially during a turn [10].
For the follower robot j, the sliding surfaces are determined based on Eqs. (5) and (6) as seen in Eqs. (21) and (22):

$$\sigma_j = \begin{bmatrix}\lambda_1 x_{ej}\\ \lambda_2 y_{ej} + \lambda_3\theta^*_{ej}\end{bmatrix}, \quad (21)$$

$$\sigma^*_j = \begin{bmatrix}-\lambda_1^2 x_{ej}\\ \lambda_1^2 y_{ej}x_{ej} - \rho(\lambda_2 y_{ej} + \lambda_3\theta^*_{\text{ej}})\end{bmatrix}, \quad (22)$$

where $\rho = \lambda_2(d_j + x_{ej}) + \lambda_3$, the elements λ_1, λ_2, λ_3 are positive constants, and $\theta^*_{\text{ej}} = \theta^*_{\text{jr}} - \theta_j$.
The control laws of the SMC and IFSMC used to obtain the control input for the follower j (v_{cj}) are determined correspondingly to Eqs. (8) and (14) appropriately, but it is necessary to underline that Eqs. (21) and (22) are used to obtain the sliding surfaces. The closed-loop control system stabilities are proven equivalently to those demonstrated for the SMC by Eqs. (9) and (10) and IFSMC by Eqs. (9) and (17). Furthermore, the formation stability is proved in a manner similar to that in [11].

3.6 Leader Control Design

The objective of the kinematic controller design for the leader robot i is to generate the velocity commands required to track a virtual robot that follows a reference trajectory defined by the posture $q_r = [x_r\ y_r\ \theta_r]^T$ and velocities $v_r = [v_{lr}\ \omega_{ar}]^T$. Since this section presents equations exclusively for the DWMR i , for a better reading flow, the subscribed "i" is not shown.
In the nonlinear systems' generic model, similar to [11], considering the term that represents the disturbances, the closed-loop system's error dynamics for trajectory tracking is expressed as in Eq. (23):

$$\begin{aligned}\dot{q}_e &= A_0(q_e,t) + B_0(q_e,t)v_c(t) + d_b(q,t)\\ \begin{bmatrix}\dot{x}_e\\ \dot{y}_e\\ \dot{\theta}^*_e\end{bmatrix} &= \begin{bmatrix}v_{lr}cos(\theta_e)\\ v_{lr}sin(\theta_e)\\ \omega^*_{ar}\end{bmatrix} + \begin{bmatrix}-1 & y_e\\ 0 & -(d+x_e)\\ 0 & -1\end{bmatrix}\begin{bmatrix}v_{lc}+\tilde{d}_{0_v}\\ \omega_{ac}+\tilde{d}_{0_\omega}\end{bmatrix},\end{aligned} \quad (23)$$

where $\theta_e = \theta_r - \theta$ and, from the inverse kinematics, as an expected motion representation in task space, the auxiliary reference angular velocity ω^*_{ar} is obtained as in Eq. (24):

$$\omega^*_{ar} = -\frac{1}{d}v_{lr}sin(\theta^*_r - \theta_r), \quad (24)$$

since the orientation of the robot i (leader) may not be the same as the orientation of the reference robot during the execution of a turning maneuver [10].
The sliding variables (sliding surfaces σ and σ^*) are chosen based on Eqs. (5 and 6) as can be verified in Eqs. (25) and (26):

$$\sigma = \begin{bmatrix}\lambda_1 x_e\\ \lambda_2 y_e + \lambda_3\theta^*_e\end{bmatrix}, \quad (25)$$

$$\sigma^* = \begin{bmatrix}-\lambda_1^2 x_e\\ \lambda_1^2 y_e x_e - [\lambda_2(d+x_e)+\lambda_3](\lambda_2 y_e + \lambda_3\theta^*_e)\end{bmatrix}, \quad (26)$$

where $\theta^*_{\text{e}} = \theta^*_{\text{r}} - \theta$.
The stability proof is similarly carried out for both the SMC and IFSMC using the same definite Lyapunov candidate function $V > 0$ as the Eq. (9). The control laws are also the same Eq. (8) for the SMC and Eq. (14) for the IFSMC to establish the convergence of the sliding manifold (Eqs. (25) and (26)). The derivative of V results in Eqs. (10) and (17) for the SMC and IFSMC, respectively, thus ensuring the sliding mode occurrence with the achievement of $\sigma(q_e,t) \to 0$, $\dot{\sigma}(q_e,t) \to 0$, $\sigma^*(q_e,t) \to 0$ and $\dot{\sigma}^*(q_e,t) \to 0$.

4. Proposed Obstacle Avoidance

Given the possibility of a scenario with unknown static obstacles during the trajectory tracking, an OA

strategy applying a reactive method is proposed for the robot i (leader in the formation control).

Considering the obstacle coordinates $(x_a,\ y_a)$ and circular-shaped obstacle avoidance area, as illustrated in Fig. 3, the relative distance from the DWMR i to the ath obstacle is defined in Eq. (27) as [30]:

$$d_{ia} = \|l_{ia}\|_2 = \sqrt{(x_a - x_i)^2 + (y_a - y_i)^2} \tag{27}$$

where $l_{ia} = [x_a - x_i\ ,\ y_a - y_i]^T$ and $\|\cdot\|_2$ is the Euclidean norm.

Some assumptions can be made in the following [7]: (i) Each mobile robot has an onboard sensing system that can detect the obstacle based on distance measurements; (ii) the obstacles are detectable so that their central coordinates are known; (iii) an obstacle is considered detected by the DWMR if $d_{ia} \leq D_{det}$, where D_{det} expresses the utmost measure interspace length reachable by the sensor coupled on the DWMR; (iv) the obstacles can be delimited by a circular area with radius r_a; (v) the obstacles are also surrounded by an avoidance area with radius $\overline{R}_d$ that must be larger than the physical obstacles, i.e., $\overline{R}_d > r_a$; (vi) It is considered as a collision occurrence when $d_{ia} \leq r_a$.

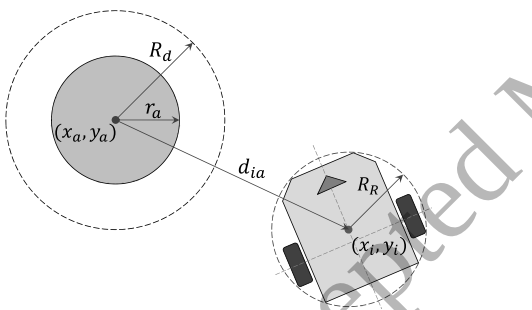

Figure 3 DWMR's relative position to an obstacle.

The avoidance area radius $\overline{R}_d$, Eq. (28), can be established taking into account the radius of obstacle r_a, the radius of the DWMR R_R and a margin of safety δ_{R_d} as [45]:

$$\overline{R}_d = r_a + R_R + \delta_{R_d}. \tag{28}$$

Some works propose to dynamically change the radius of the OA area that circumvents the obstacle, even if its dimension does not vary, as in [46, 47]. The possibility of expanding the $\overline{R}_d$ value is such that it allows the DWMR trajectory to be affected in advance upon detection of an obstacle, making the task of avoiding collisions less arduous [48]. In this work, based on the proposal of [47], with the expectation of obtaining a safe and smooth trajectory for the OA, an avoidance radius R_d is introduced, which is adaptively expanded depending on the velocity and direction of movement of the DWMR concerning the obstacle's relative position. When the DWMR is far from an obstacle, there is no immediate need to increase the safety radius, allowing greater focus on trajectory tracking performance. However,as the robot approaches the obstacle and the relative distance decreases, safety becomes a higher priority, making it appropriate to expand the safety radius more significantly. Also, the faster the DWMR is relative to the obstacle, for safer and smoother movement, the more appropriate it may be to increase the radius. As this relative velocity decreases, the expansion can be smaller [47].

Thus, there is an inverse proportionality relationship between the enlargement of the obstacle avoidance radius and the distance from the DWMR to the obstacle, as well as a direct proportion of the expansion of the radius with the relative velocity. Thus, the avoidance region radius R_d with a self-adaptive expansion radius r_d can be defined by Eqs. (29) and (30) as [47]:

$$R_d = \overline{R}_d + r_d \tag{29}$$

$$r_d = \frac{\kappa |v_{ia}|}{\gamma^{\varrho d_{ia}}}, \tag{30}$$

where κ is a gain value, ϱ is a parameter used to adjust the denominator value, which is set as $\gamma^{\varrho d_{ia}}$ to make the reactive expansion radius grow ascendingly when the relative distance from the DWMR i to obstacle a, d_{ia}, becomes smaller. Defining the relative velocity between the DWMR and the obstacle as $v_{l_i} - v_{l_a}$, following [47], then $v_{ia} = (v_{l_i} - v_{l_a})cos(\phi)$ is considered the relative velocity's projection over the relative distance. Since only static obstacles are considered, so $v_{l_a} = 0$. Thus, v_{ia} can be denoted as in Eqs. (31) and (32):

$$v_{ia} = v_{l_i} cos(\phi) \tag{31}$$

in which

$$\phi = \begin{cases} \theta_i - \theta_{la} & \text{if } \theta_{la} < \theta_i \\ (\theta_i - \theta_{la}) + 2\pi & \text{otherwise} \end{cases}, \tag{32}$$

where θ_{la} designates the angle between the obstacle and the DWMR, given by Eq. (33):

$$\theta_{la} = atan2(y_a - y_i,\ x_a - x_i). \tag{33}$$

It is advisable to limit the avoidance radius R_d so that it does not increase too much, regarding the maximum sensing range of the DWMR, for example. For this, denoting a maximum bound value as $\overline{R}_b$, the radius R_d (Eq. (29)) can be bounded considering it as in Eq. (34):

$$R_d = min(\overline{R}_b, \overline{R}_d + r_d). \tag{34}$$

The reactive OA method is based on the one presented in [7], which differs in that it involves switching between a classic backstepping controller and the OA controller. In contrast, the present work maintains an unaltered control structure, focusing instead on recalculating the reference trajectory online for obstacle avoidance (as usual in some reactive OA approaches such as [49]), consequently modifying the tracking error dynamics and then influencing the generated sliding surfaces.

The OA mode is activated when the DWMR is tracking the original reference trajectory and its relative distance to obstacle (d_{ia}), Eq. (35), is such that:

$$r_a < d_{ia} \leq R_d. \tag{35}$$

To conduct the obstacle avoidance, a term U_b is set to guide the DWMR in a certain steering way as in Eq. (36) [7]:

$$U_b = l_{ia} - R_d \frac{1}{d_{ia}} l_{ia}. \tag{36}$$

Therefore, it can be noted that U_b is a vector directed towards the obstacle when $d_{ia} > R_d$ and directed away from the obstacle when $d_{ia} < R_d$, becoming zero when $d_{ia} = R_d$. It is also expected that the DWMR will tend to move in a parallel direction around the margins of the obstacle avoidance area. This, an additional vector U_f is established as in Eqs. (37) and (38) [7]:

$$U_f = R_f l_{ia} \tag{37}$$

where

$$R_f = \begin{bmatrix} cos(\alpha) & -sin(\alpha) \\ sin(\alpha) & cos(\alpha) \end{bmatrix}. \tag{38}$$

The Eq. (38) determines R_f as a rotation matrix applied to obtain the vector U_f from the alteration of the vector l_{ia}, being the term α defined by Eq. (39) [7]:

$$\alpha = \begin{cases} \pi/2, & \theta_i \geq \theta_{la} \\ -\pi/2, & \theta_i < \theta_{la} \end{cases} \tag{39}$$

The Eqs. (33) and (39) are intended to settle the swiftest route for the DWMR to get around the obstacle. When $\theta_i > \theta_{la}$, one has $\alpha = \pi/2$ and the vector U_f can be attained from rotation of the vector l_{ia} spinning α radians counterclockwise. With the term α remaining fixed during OA, the DWMR goes in its left direction to contour the obstacle. With a combination of the vectors U_b and U_f, Eqs. (36) and (37), a blending vector is obtained as in Eq. (40) [7]:

$$U = U_b + U_f = \begin{bmatrix} U_x & U_y \end{bmatrix}^T. \tag{40}$$

Thus, the desired motion direction of the DWMR can be obtained based on the angle between the vector U and the positive direction of the x-axis, as can be seen in Eq. (41) [7]:

$$\theta_{r_{OA}} = atan2(U_y,\, U_x) \tag{41}$$

where U_x and U_y are, correspondingly, the components on the x and y axes of the vector U.

The reference linear velocity remains the same in [7], and does not change when going from original trajectory tracking to OA mode. In this work, it was chosen to reduce the linear velocity during the OA as recommended in [32] for safe avoidance. Similarly to [32], a parameter $0 < \rho_v < 1$ is considered to decrease the reference linear velocity's amplitude when the DWMR is in the obstacle avoidance mode as in Eq. (42):

$$v_{lr_{OA}} = \rho_v v_{lr}. \tag{42}$$

If $\rho_v = 1$, the linear velocity remains the same as in regular trajectory tracking. It is worth noting that switching between different reference velocities can introduce discontinuities, particularly when the DWMR slows down to avoid an obstacle and then speeds up to return to the original reference velocity. However, for the sake of simplicity, this approach was adopted in this work.

Considering the inverse kinematics and the reference orientation $\theta_{r_{OA}}$ by Eq. (41), the auxiliary reference angular velocity, Eq. (24), when in the OA mode, is redefined in Eq. (43) as:

$$\omega^*_{ar_{OA}} = -\frac{1}{d_i} v_{lr_{OA}} sin(\theta^*_{r_{OA}} - \theta_{r_{OA}})\,. \tag{43}$$

Thereby, it can be seen that the OA occurs mainly due to a modification of the original desired DWMR's orientation, with a just reduction in the linear velocity. Thus, basically, for a better understanding, $q_{r,tt} = [x_{r,tt}\ y_{r,tt}\ \theta_{r,tt}]^T$ and $v_{r,tt} = [v_{lr,tt}\ \omega_{ar,tt}]^T$ can be denoted as the original trajectory tracking reference posture and velocities respectively, and $q_{r,oa} = [x_{r,oa}\ y_{r,oa}\ \theta_{r,oa}]^T$ and $v_{r,oa} = [v_{lr,oa}\ \omega_{ar,oa}]^T$ as the reference posture and velocities in the OA mode, respectively. Only one mode is active at a time, i.e., the reference motion (q_r, v_r) will assume only ($q_{r,tt}$, $v_{r,tt}$) or ($q_{r,oa}$, $v_{r,oa}$). If the condition determined by Eq. (35) is met, OA mode is activated, otherwise, the desired motion is prescribed by the original trajectory tracking. In this way, in OA mode, the posture error is described similarly as in [11] with $q_r = q_{r,oa}$, for which Eq. (41) is considered, and the error dynamics is similar to Eq. (23) considering Eq. (43), based on which the sliding surfaces in OA mode are obtained similarly to the process for Eqs. (25) and (26). With these sliding surfaces, as the control structure remains the same, the SMC and IFSMC control laws are established similarly to Eqs. (8) and (14), respectively.

Variables c_{tt} and c_{oa} can be established to represent the mode state, which can be 1 (one) if it is active and 0 (zero) otherwise. So, a total Lyapunov function for the kinematic controllers of the leader robot i can be defined in Eq. (44) as:

$$V_t = c_{tt}V_{tt} + c_{oa}V_{oa}\ , \tag{44}$$

where V_{tt} and V_{oa} are determined by the respective considered kinematic tracking controller, such as Eq. (9). The total Lyapunov function's time derivative is denoted as in Eq. (45):

$$\dot{V}_t = c_{tt}\dot{V}_{tt} + c_{oa}\dot{V}_{oa} \tag{45}$$

where similarly $\dot{V}_{tt}$ and $\dot{V}_{oa}$ are established as Eqs. (10) and (17) for SMC and IFSMC, respectively.
Accordingly, this means that, depending on which mode is active, $V_t = V_{tt}$ or $V_t = V_{oa}$, and $\dot{V}_t = \dot{V}_{tt}$ or $\dot{V}_t = \dot{V}_{oa}$, being the proofs that $V_{tt} > 0$, $V_{oa} > 0$, $\dot{V}_{tt} \leq 0$ and $\dot{V}_{oa} \leq 0$ demonstrated similarly in the stability analyses performed in the Sections 3.1 and 3.3. Note also that the convergence of the original to the OA reference trajectory or vice versa is not treated here, assuming smoothness and convergence of the DWMR's orientation to near surroundings of reference orientation. Thus, updating the reference can temporarily degenerate the tracking performance, which can be seen as a disturbance effect. Thus, it is up to the proposed robust controller to handle the tracking errors resulting from the OA.

5. Implementation results

5.1 Simulation results in Matlab/Simulink

Results of trajectory tracking and formation control obtained from simulations performed in the software Matlab/Simulink (version R2024b), considering 200s of total simulation time and the Dormand-Prince solver, are presented in this section. For the PD dynamic controller of the DWMRs leader i and followers j, the control law was settled by Eq. (18) (which can be expressed in the time domain as $\tau = \overline{E}(q)^{-1}\left(k_d\dot{v}_e + k_p v_e\right)$). For the kinematic controllers SMC and IFSMC, the control laws were determined respectively by the Eqs. (8) and (14).
For the simulations, based on [35], a configuration model was considered (in space-state with limitations and with structural uncertainties represented by actuator dynamics) of the PowerBot robot, which has an internal PD controller embedded in its closed platform to track v_e and ω_e as input with 5 ms of sampling time. Since generalized forces (that must be converted into control torques in the configuration model) acting on the inertia center of the robot are generated, the PD controller's signals need to be multiplied by a matrix T_v^{-1}, which relates wheels' torques with generalized torques, given as [35]: $T_v^{-1} = \left[\frac{1}{r}\ \ \frac{b}{r};\ \frac{1}{r}\ \ \frac{-b}{r}\right]$, where $2b$ is the PowerBot's width.
The PD control has its gains with the following values $k_{p_v} = 40$, $k_{p_\omega} = 40$, $k_{d_v} = 20$, $k_{d_\omega} = 20$, $N_v = 10$ and $N_\omega = 10$ according to the manufacturer "MobileRobots Inc." as well as obtaining a fair time of response under the presence of unmodeled nonlinearities and averting overdone oscillations [35, 44].
The leader DWMR must track an eight-shaped reference trajectory with formulation as in [11, 36, 37]. Its course is characterized by curves, accelerations, and decelerations over time, with change between 0.33 m/s to 1.05 m/s for linear velocity and -0.18 rad/s to 0.18 rad/s for angular velocity.
The values of the desired separation distance L_{ijd} and the desired bearing angle Ψ_{ijd}, presented in Table 2, determine the considered triangular formation shape.

Table 2 Values of Ψ_{ijd} and L_{ijd} for followers.

	Ψ_{ijd}	L_{ijd}
Follower 1	$(3/4)\pi$ rad	1.1 m
Follower 2	$-(3/4)\pi$ rad	1.1 m

Table 3 shows the posture of the DWMRs and reference at $t = 0$ and the parameter d of the formation robots. The gains g_v and g_ω of the SMC and standard parameters of the kinematic controllers are shown in Table 4. Specific gains of the IFSMC k_h and k_s, have their values presented in Table 5.

Table 3 Posture at $t = 0$ and values d of the robots.

	x_0	y_0	θ_0	d
Reference	0	0	$\pi/2$	0
Leader	-1	1	0	0.1
Follower 1	-3.5	3	0	0.4
Follower 2	-3	-1	0	0.4

For the FIS used to compute the function $f(\sigma^*, \dot{\sigma}^*)$, the input MFs' parameters are shown in Table 6 and output MFs' ones, in Table 7, remembering that the MFs were calculated according to Eq. (16).

Table 4 Kinematic controller SMC gains.

Gains	λ_1	λ_2	λ_3	p_v	p_ω	g_v	g_ω
Leader	0.6	0.6	0.3	0.1	0.1	0.1	0.1
Follower 1	0.6	0.6	0.3	0.1	0.1	0.1	0.1
Follower 2	0.6	0.6	0.3	0.1	0.1	0.1	0.1

There is no exact method to choose the MFs, as it is usual to look at the distribution of data. A widely

Table 5 Gains k_h and k_s for IFSMC.

Gains	k_{h_v}	k_{s_v}	k_{h_ω}	k_{s_ω}
Leader	0.10	0.55	0.10	0.55
Follower 1	0.10	0.55	0.10	0.55
Follower 2	0.10	0.55	0.10	0.55

Table 6 Input MFs parameters.

	σ^*			$\dot{\sigma}^*$		
	α_1	α_2	α_3	α_1	α_2	α_3
NB	$-\infty$	-0.030	-0.015	$-\infty$	-0.50	-0.25
NS	-0.030	-0.015	0.000	-0.50	-0.25	0.00
ZO	-0.015	0.000	0.015	-0.25	0.00	0.25
PS	0.000	0.015	0.030	0.00	0.25	0.50
PB	0.015	0.030	∞	0.25	0.50	∞

Table 7 Output MFs parameters.

	f_v			f_ω		
	α_1	α_2	α_3	α_1	α_2	α_3
NB	$-\infty$	-1.00	-0.66	$-\infty$	-1.00	-0.66
NM	-1.00	-0.66	-0.33	-1.00	-0.66	-0.33
NS	-0.66	-0.33	0.00	-0.66	-0.33	0.00
ZO	-0.33	0.00	0.09	-0.33	0.00	0.09
PS	0.00	0.09	0.18	0.00	0.09	0.18
PM	0.09	0.18	∞	0.09	0.18	∞

adopted shape, especially in implementation with real-time operating requirements, is the triangular one, due to its simplicity and intuitiveness, being advisable to use symmetrical triangles with 50% overlap and then make adjustments if necessary [50].
Some additional observations can be made. The values of k_{h_v} and k_{h_ω} are set equal to the gains g_v and g_ω to enable a direct comparison between the IFSMC and the SMC approaches, and to verify the adaptive gain regulation capability of the proposed IFSMC. Moreover, with the terms k_h and k_s established, it is suitable to choose the output MFs parameters, mostly related to center values of Eq. (15), taking into account the feasible bounds of f_n according to the stability analysis based on Eq. (17).
The Matlab/Simulink tools *Simulink Design Optimization* and *Response Optimization* can be used to optimize constant parameters that have no specification, with manual fine-tuning when necessary, as described in [51]. For example, with k_h set, the value of k_s can be determined via an optimization tool, establishing how much G_{AIS} can increase. Attention is also needed on how much it can reduce. So, to avoid $G_{AIS} < 0$, a minimum value $0 < \overline{G}_{AIS} < k_h$ can be specified, thus an alternative upper bound for f can be as $f^+ = (k_h - \overline{G}_{AIS})/k_s$.
The kinematic controllers' compensation capacity, under incidence of uncertainties and disturbances similar to those considered in [34], is verified by performing simulations taking into account changes in DWMR's mass and rotational inertia (at 40 to 160 seconds of simulation time), and also nonlinearities caused by friction (during the 200 seconds of simulation). External disturbances with different behaviors are also introduced into the system in interleaved time (as sinusoidal signals at 3 to 20 seconds and 100 to 120 seconds and continuous signals at 50 to 70 seconds and 150 to 170 seconds).
For the case with OA, the following was considered: $\rho_v = 0.1$, obstacles of radius $r_a = 0.5$ m, the DWMR's radius approximately $R_R = 0.56$ m and a security margin $\delta_{R_d} = 1.25$ m. The parameters for the variable avoidance radius R_d are shown in Table 8. The coordinates of the obstacles were established similarly to [30], as shown in Table 9, trying to position them in different ways along the trajectory (with the edge on the trajectory, in the middle, with part of the obstacle covering it). Another point that will be possible to note is that the obstacles coincide with the occurrence of the applied disturbances' effects (at the beginning, middle, and end of the incidence of the disturbances for each obstacle, respectively).

Table 8 Parameters for the variable avoidance region radius R_d.

$\overline{R}_d$ [m]	$\overline{R}_b$ [m]	κ	γ	ϱ
2.31	5.00	5.00	2.00	1.00

Table 9 Obstacles coordinates.

	Obstacle 1	Obstacle 2	Obstacle 3
x_a	0.00	8.00	-14.50
y_a	15.50	-4.25	-11.25

To measure the chattering level, $|\dot{v}_c|$ is adopted [52]. As commonly used in the literature, the root mean square errors (RMSEs) are used as a performance evaluation method, being given by $RMSE(x) = \left[\frac{1}{T}\sum_{k=1}^{T} x_k^2\right]^{1/2}$, where T denotes the number of samples and x_k, the error in the k-th sample [34, 35].

Table 10 RMSEs – Simulation results.

		x_e	y_e	θ_e
Leader	SMC	5.3006	3.2241	0.7044
	IFSMC	1.3891	0.5368	0.3473
Follower 1	SMC	0.7684	2.2650	3.8290
	IFSMC	0.1727	0.0826	0.0359
Follower 2	SMC	0.6396	1.0648	0.4074
	IFSMC	0.1155	0.0870	0.0286

5.1.1 Simulation results of the SMC

Results obtained from the simulation of the SMC are presented in Figs. 4 to 6. Observing Fig. 4, it can be stated that the gains were not sufficient to compensate for the auxiliary velocity tracking errors (seen as disturbances in the kinematics), and the closed-loop control system showed an inability to ensure effectiveness. This, in turn, affected the stability and performance of the tracking and formation control, given that the measured separation and bearing did not converge to the desired values, resulting in evident errors as noted in Fig. 5. Greater RMSEs are verified in Table 10.

Still, in Fig. 4, the avoidance area is represented by the circle, considering the fixed minimum radius $\overline{R}_d$. It is also worth noting that, although the robot continues to avoid obstacles, a collision does occur at some point. Thus, the maintenance of the robustness and attractiveness of a conventional SMC is related not only to a suitable selection of sliding surfaces but also to sufficient gain values, which is related to knowing the boundary of the disturbances in advance. Moreover , the chattering occurrence is quite evident and relevant or significant in Fig. 6, which is undesirable.

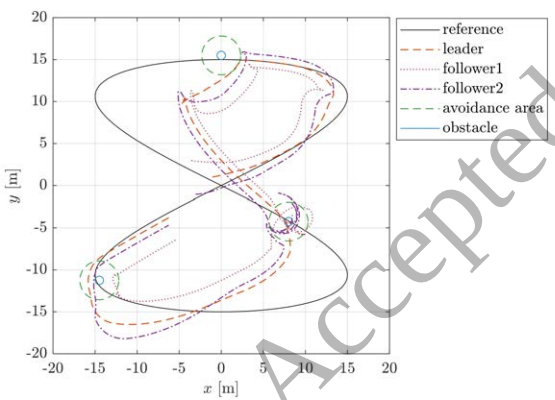

Figure 4 Trajectory tracking, formation, and OA (SMC).

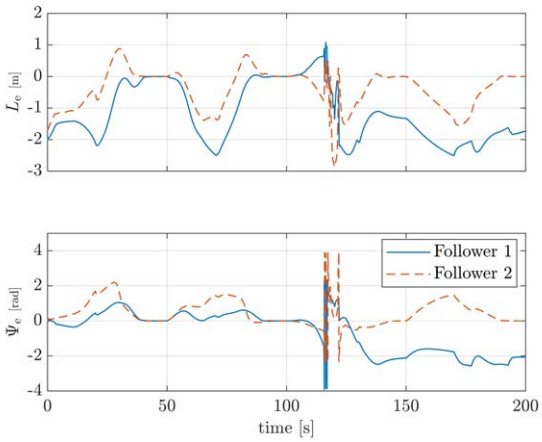

Figure 5 Separation and bearing errors (SMC).

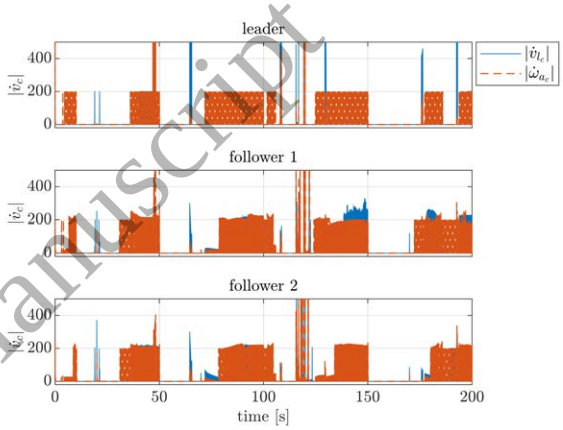

Figure 6 Chattering measure (SMC).

5.1.2 Simulation results of the IFSMC

Figs. 7 to 22 show the results for IFSMC, which ensured stability and accuracy in trajectory tracking, formation, and OA, as shown in Fig. 7. The sliding surfaces and their derivatives in Figs. 8 and 9 show the attainment of the sliding manifolds (σ, σ^*, $\dot{\sigma}$ and $\dot{\sigma}^*$ tend to zero), achieving the control aims. The compensation efforts of the IFSMC can be seen in Figs. 10, 11 and 12, , where compensatory signals are generated by the sliding mode portion of Eq. (14) (see cp2 of Eq. (8)) with opposite behavior to cancel the effects of the uncertainties and disturbances, including those derived from the OA process. The separation and bearing errors tend to zero, viewing Fig. 13, thus confirming that the wished formation was performed. In addition, a smoother behavior than the SMC is observed in Fig. 14, in which the chattering phenomenon was mitigated or attenuated significantly. As shown in Fig. 15, due to the AIS, the gains of the sliding mode control portion are adaptively regulated, increasing when it is necessary to act against the disturbances, in an attempt to eliminate observed errors, or decreasing to reduce the control efforts and lead to system stability.

Moreover, Fig. 16 displays the blending vectors generated by the OA method, Figs. 17, 18 and 19 show the variable avoidance radius for each obstacle, Figs. 20, 21 and 22, the relative distances from the DWMRs to obstacles. Follower 2, which is just following the leader, is the one that ends up getting closest, passing at a distance of 0.45 m, 0.02 m, and 0.21 m from the obstacles as seen in Fig. 22.

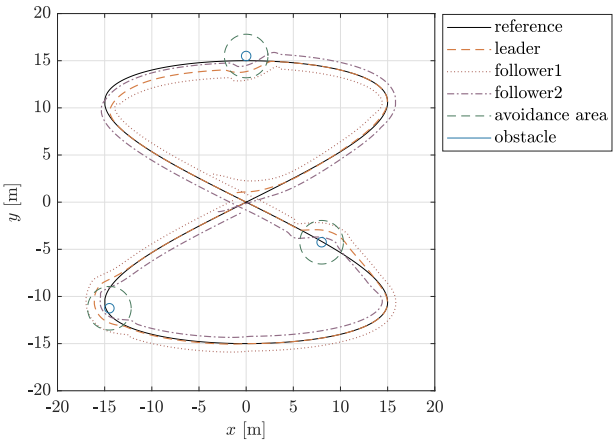

Figure 7 Trajectory tracking, formation, and OA (IFSMC).

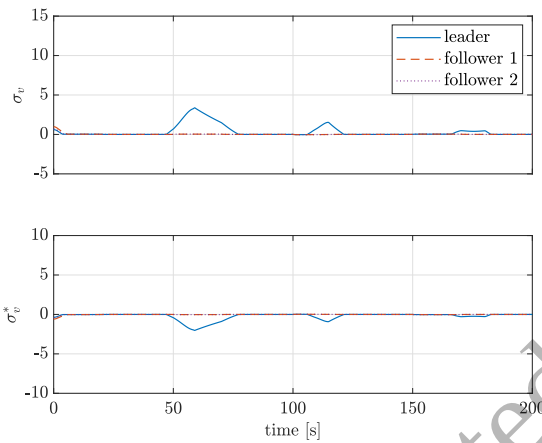

Figure 8 Sliding surfaces σ_v and σ_v^* (IFSMC).

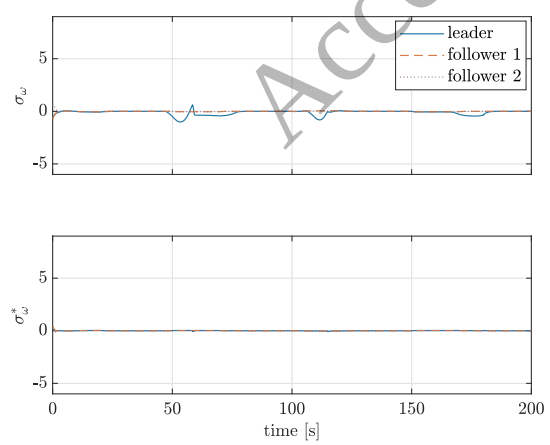

Figure 9 Sliding surfaces σ_ω and σ_ω^* (IFSMC).

5.2 Simulation results in Gazebo

To analyze the accuracy of the proposed formation tracking control with OA, results obtained from

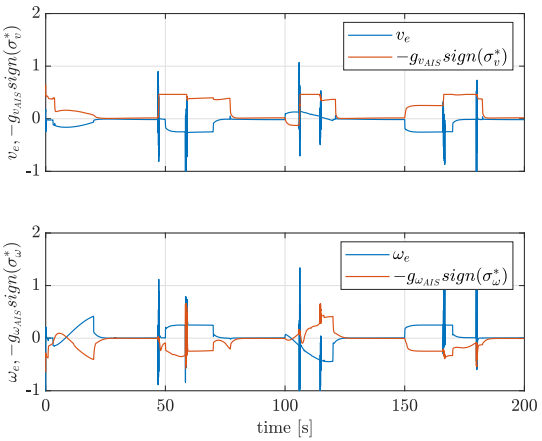

Figure 10 Leader: Compensations of v_e and ω_e (seen as disturbances) by the sliding mode control portion (IFSMC).

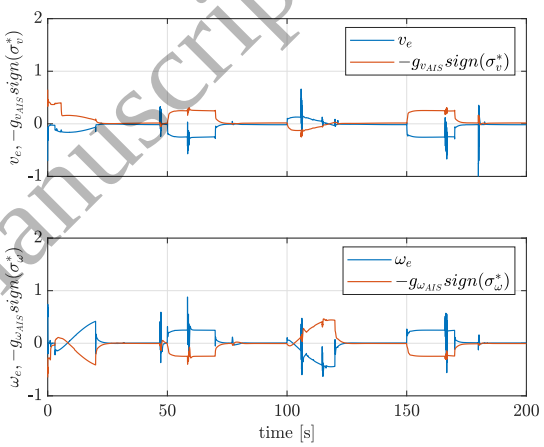

Figure 11 Follower 1: Compensations of v_e and ω_e (seen as disturbances) by the sliding mode control portion (IFSMC).

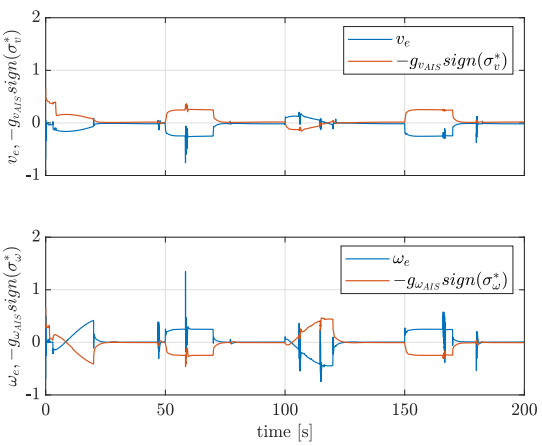

Figure 12 Follower 2: Compensations of v_e and ω_e (seen as disturbances) by the sliding mode control portion (IFSMC).

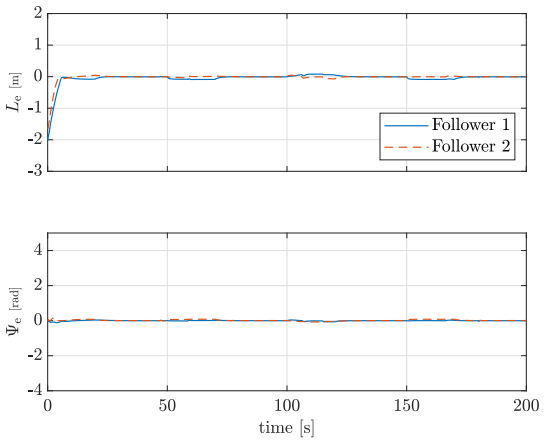

Figure 13 Separation and bearing errors (IFSMC).

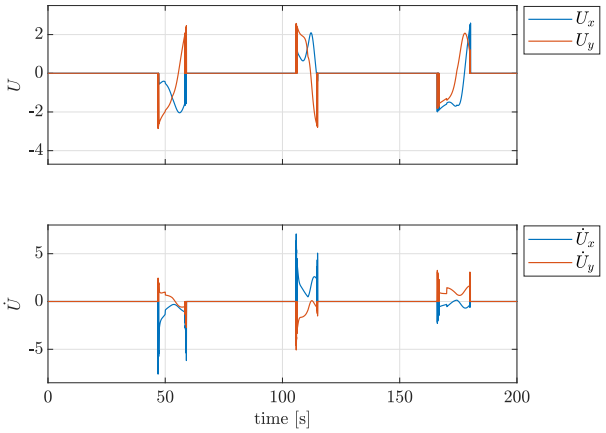

Figure 16 OA blending vectors (IFSMC).

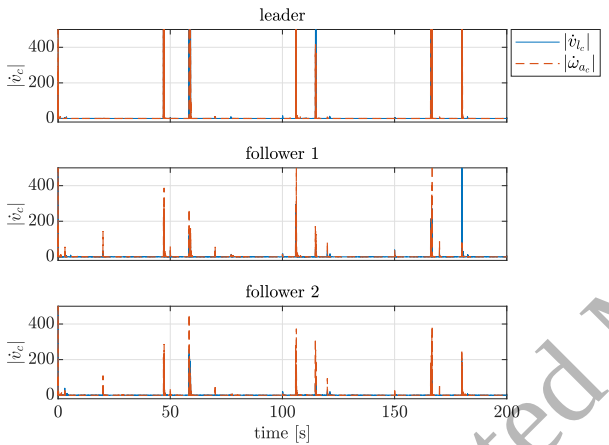

Figure 14 Chattering measure (IFSMC).

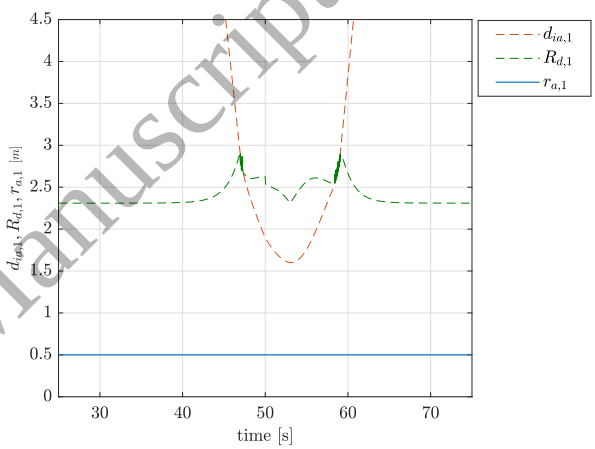

Figure 17 Variable radius $R_{d,1}$ with zoom (IFSMC).

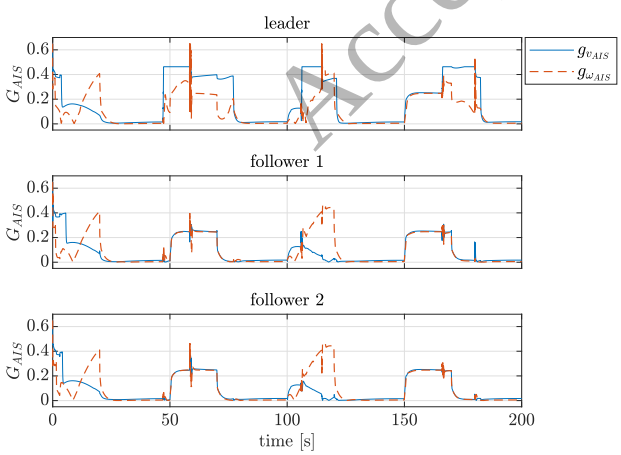

Figure 15 AIS gain G_{AIS} (IFSMC).

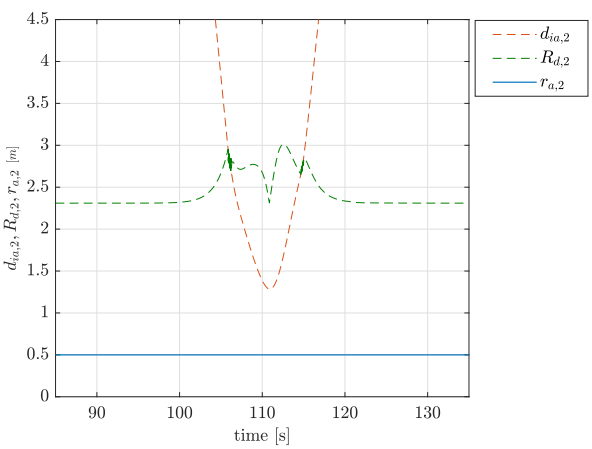

Figure 18 Variable radius $R_{d,2}$ with zoom (IFSMC).

simulation for the IFSMC were carried out using the Gazebo Classic simulator (version 11.14), an open-source option for emulating physical models that can be connected to Matlab/Simulink, where the proposed algorithm has been implemented. In this prototyping simulator, the obstacles are considered

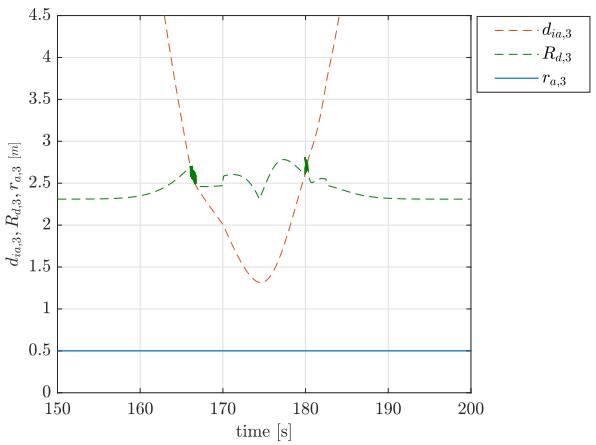

Figure 19 Variable radius $R_{d,3}$ with zoom (IFSMC).

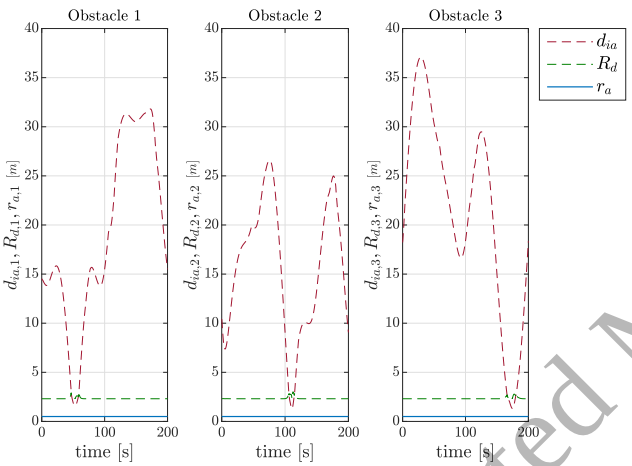

Figure 20 Relative distance from leader to obstacles (IFSMC).

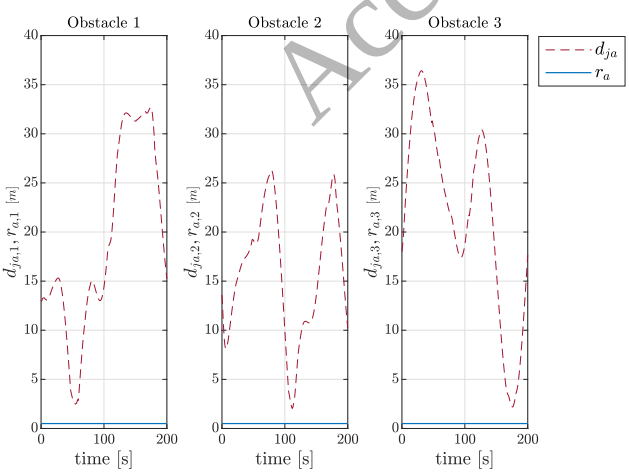

Figure 21 Relative distance from follower 1 to obstacles (IFSMC).

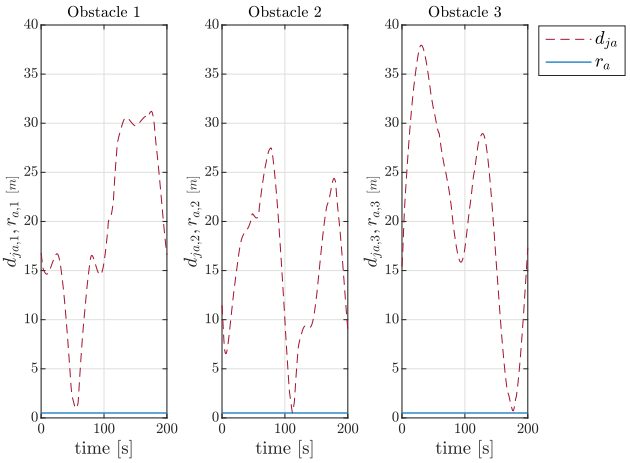

Figure 22 Relative distance from follower 2 to obstacles (IFSMC).

virtual, and the nonlinearities and uncertainties are just derived from the robot's model in the Gazebo, with the model of the PowerBot DWMR being considered. The obtained RMSEs are shown in Table 11 and Figs. 23 to 38 are presented as the results of the simulations using Gazebo. These RMSEs and results do not differ much from the behavior observed in simulation results of Matlab/Simulink, so the same observations in Section 5.1.2 must be considered here, with relevant chattering mitigation and the proposed control aims accomplishment, thus obtaining satisfactory performance in the formation tracking control with OA.

In short, an acceptable control accuracy in the trajectory tracking, formation, and OA was verified (Fig. 23); as expected, the sliding surfaces and their derivatives tended to zero (Figs. 24 and 25), thereby guaranteeing the existence of the sliding mode and, consequently. ensuring Lyapunov's stability. The compensations of the uncertainties and disturbances— both for the leader (Fig. 26) and the followers (Figs. 27 and 28)— were realized by the respective sliding mode control portions. Fig. 29 certifies that the desired formation was maintained since the separation-bearing errors tended to zero. Moreover, the chattering level was significantly attenuated in the control efforts provided by the IFSMC (Fig. 30). Fig. 31 represents the gains of the sliding mode control portion adaptively regulated by the procedure for activating and restricting the inhibitory effect of the nonlinear function $f(\cdot)$ of the AIS, thus not requiring a prior information about the boundary of the disturbances. Finally, the proposed OA method worked adequately, as can be seen in Figs. 32 to 38.

Table 11 RMSEs – Simulation with Gazebo (IFSMC).

	$RMSE(x_e)$	$RMSE(y_e)$	$RMSE(\theta_e)$
Leader	0.6800	0.5802	0.3565
Follower 1	0.1329	0.1783	0.0465
Follower 2	0.1148	0.0782	0.0273

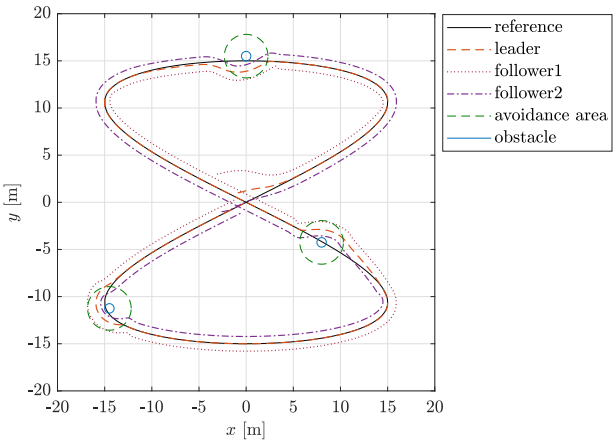

Figure 23 Trajectory tracking, formation, and OA (IFSMC) – Simulation with Gazebo.

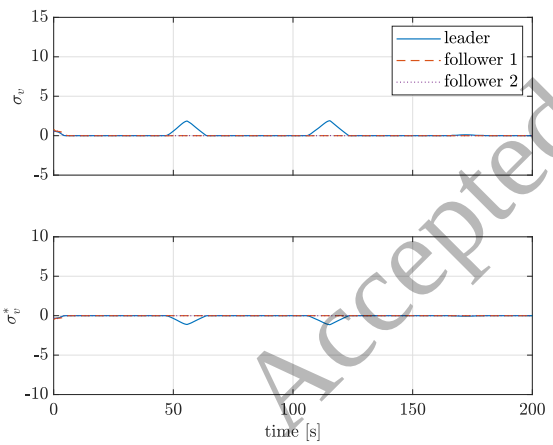

Figure 24 Sliding surfaces σ_v and σ_v^* (IFSMC) – Simulation with Gazebo.

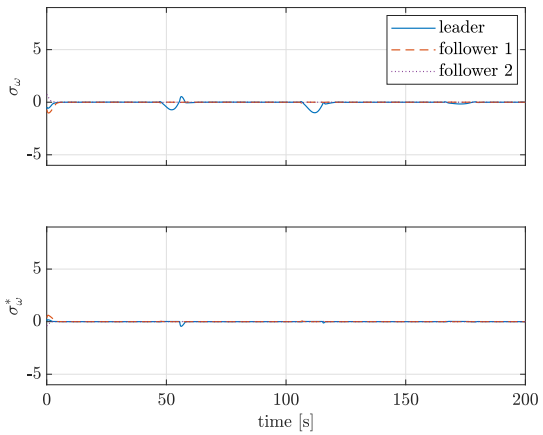

Figure 25 Sliding surfaces σ_ω and σ_ω^* (IFSMC) – Simulation with Gazebo.

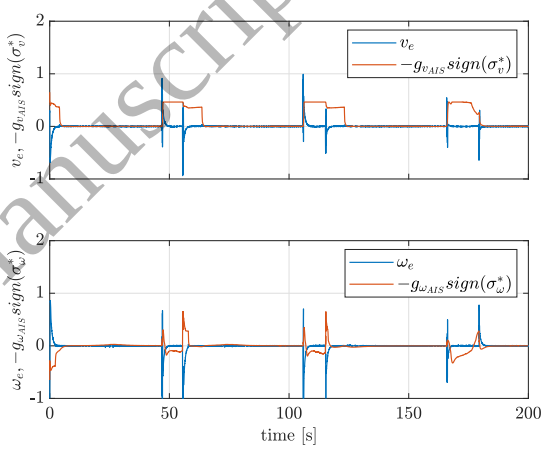

Figure 26 Leader: Compensations of v_e and ω_e (seen as disturbances) by the sliding mode control portion (IFSMC) – Simulation with Gazebo.

6. Conclusion

This article proposed the combination of a formation control scheme employing the leader-follower separation-bearing model, trajectory tracking, and obstacle avoidance, considering the existence of uncertainties and matched disturbances on the DWMRs. The IFSMC is proposed to control the kinematics. It is inspired by the adaptive humoral immunity, enabling an adaptable regulation of sliding mode portion gains, providing alleviation of the control efforts and also the capacity of the control system to deal with auxiliary velocity tracking errors originated from dynamics and seen as uncertainties and disturbances for the kinematics, with no previous knowledge of their magnitude. The proposed control scheme also addresses the obstacle avoidance problem. The proof of the stability of the proposed IFSMC in closed-loop was analyzed using Lyapunov's theory.

It is worth emphasizing that, although the proposed method retains the discontinuous signum function characteristic of classical SMC—thus preserving the invariance principle and robustness—it distinguishes itself by significantly reducing, or even eliminating, chattering solely through gain regulation via the AIS mechanism.

For future work, different models of mobile robots

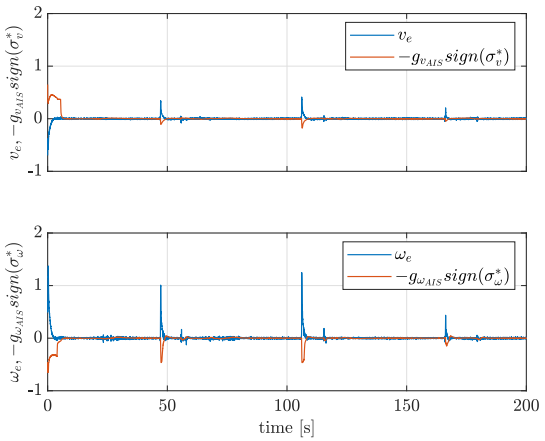

Figure 27 Follower 1: Compensations of v_e and ω_e (seen as disturbances) by the sliding mode control portion (IFSMC) – Simulation with Gazebo.

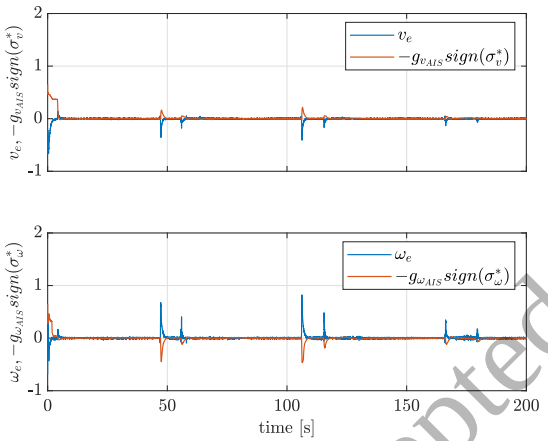

Figure 28 Follower 2: Compensations of v_e and ω_e (seen as disturbances) by the sliding mode control portion (IFSMC) – Simulation with Gazebo.

and even new coordinates, as is the case with unmanned aerial vehicles, could be considered. Furthermore, the present work opens up a range of possibilities to extend studies on trajectory tracking with obstacle avoidance, such as considering other OA methods or a flexible formation, the treatment of dynamic obstacle avoidance problems, or different obstacle configurations (wall type, concave shape, forming a cluttered environment), avoidance of inter-collision between DWMRs and the obstacle avoidance by the followers DWMRs as well, since they are still subject to a possible collision, being a prospective area that remains unexplored. Future research considering the variable avoidance radius may be a way to address this challenge.

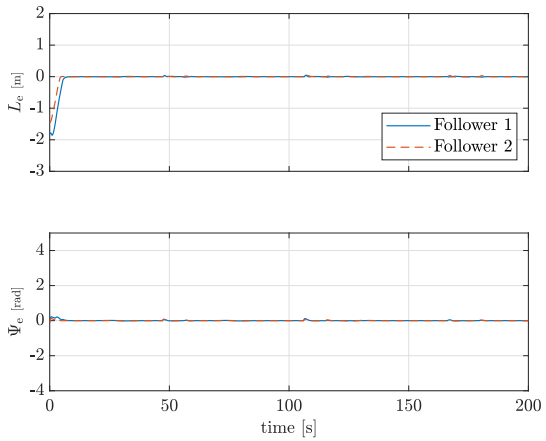

Figure 29 Separation and bearing errors (IFSMC) – Simulation with Gazebo.

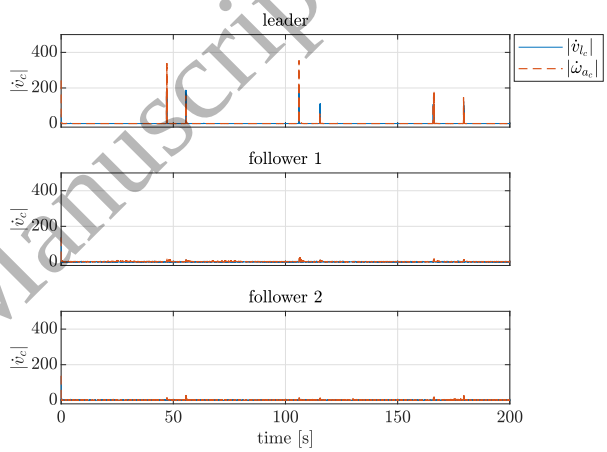

Figure 30 Chattering measure (IFSMC) – Simulation with Gazebo.

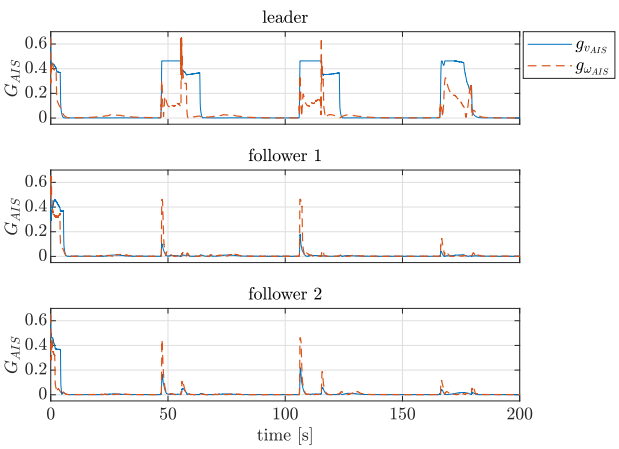

Figure 31 AIS gain G_{AIS} (IFSMC) – Simulation with Gazebo.

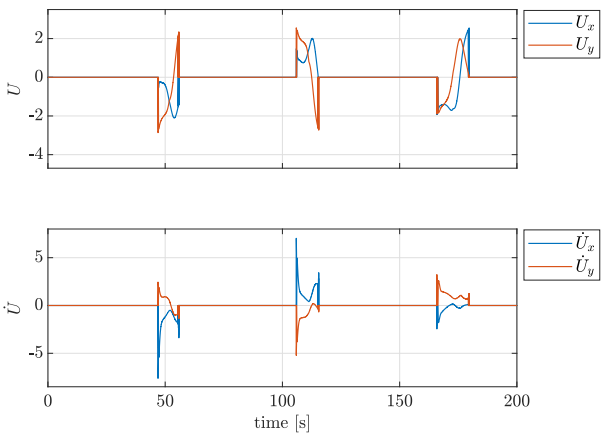

Figure 32 OA blending vectors (IFSMC) – Simulation with Gazebo.

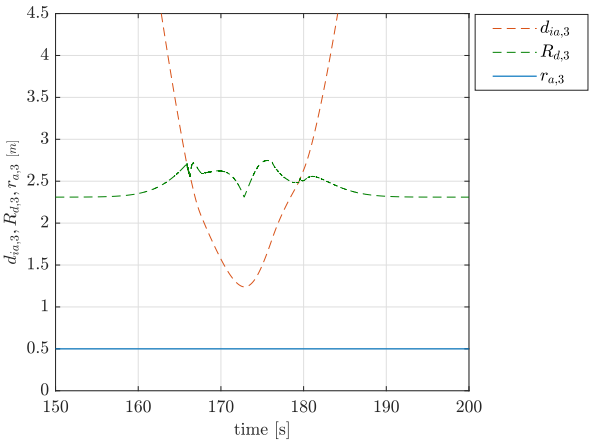

Figure 35 Variable radius $R_{d,3}$ with zoom (IFSMC) – Simulation with Gazebo.

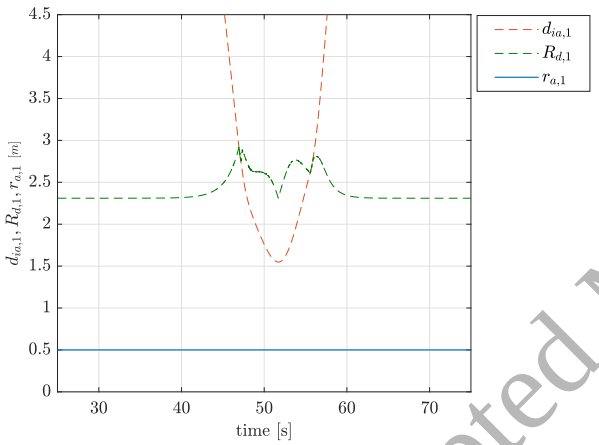

Figure 33 Variable radius $R_{d,1}$ with zoom (IFSMC) – Simulation with Gazebo.

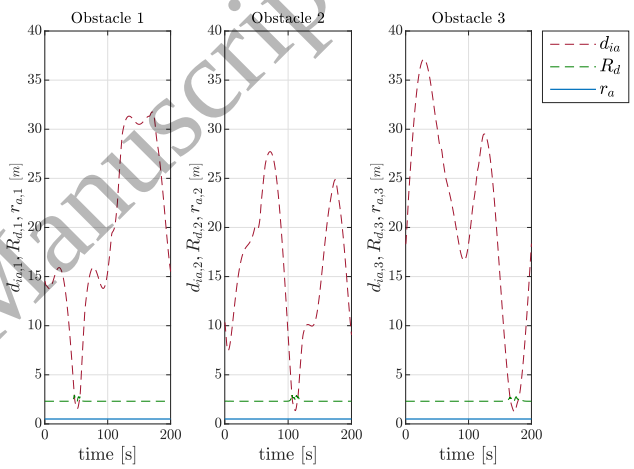

Figure 36 Relative distance from leader to obstacles (IFSMC) – Simulation with Gazebo.

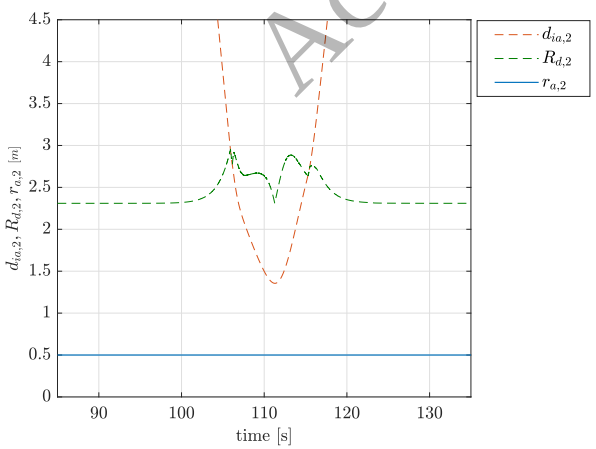

Figure 34 Variable radius $R_{d,2}$ with zoom (IFSMC) – Simulation with Gazebo.

7. Declaration of competing interest

The authors reported that there were no conflicts or competing interests.

8. Acknowledgements

This research was financed in part by the Coordenação de Aperfeiçoamento de Pessoal de Nível Superior - Brasil (CAPES) - Finance Code 001

9. Author contributions

The authors declare that they have contributed equally to the paper. **Willy John Nakamura Goto:**

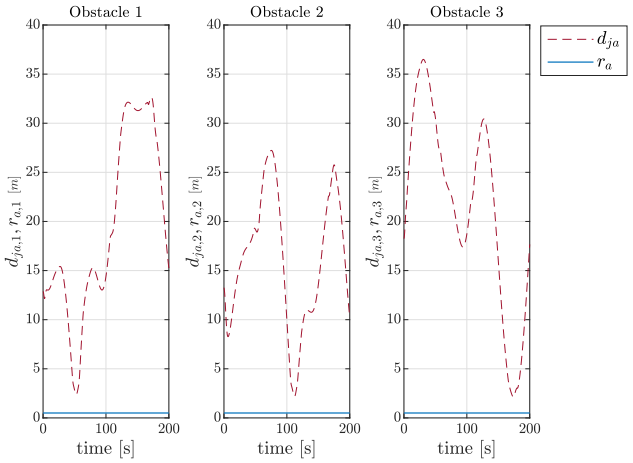

Figure 37 Relative distance from follower 1 to obstacles (IFSMC) – Simulation with Gazebo.

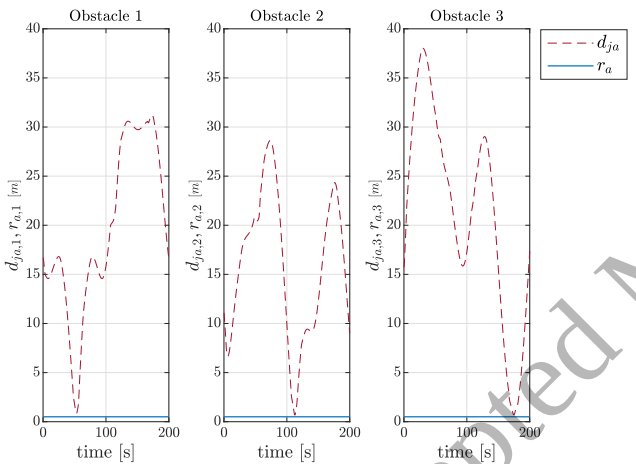

Figure 38 Relative distance from follower 2 to obstacles (IFSMC) – Simulation with Gazebo.

Investigation, Conceptualization, Development of the research proposal, Simulation, Writing. **Douglas Wildgrube Bertol:** Investigation, Conceptualization, Research proposal development, Simulation, Writing. **Nardênio Almeida Martins.:** Investigation, Conceptualization, Research proposal development, Simulation, Supervision, and Writing.

References

[1] X. V. Wang and L. Wang, "A literature survey of the robotic technologies during the covid-19 pandemic," *Journal of Manufacturing Systems*, vol. 60, pp. 823–836, 2021.

[2] Iswanto, A. Ma'arif, N. Raharja, G. Supangkat, F. Arofiati, R. Sekhar, and D. Rijalusalam, "Pid-based with odometry for trajectory tracking control on four-wheel omnidirectional covid-19 aromatherapy robot," *Emerging Science Journal*, vol. 5, pp. 157–181, 11 2021.

[3] S. Moorthy and Y. H. Joo, "Formation control and tracking of mobile robots using distributed estimators and a biologically inspired approach," *Journal of Electrical Engineering & Technology*, vol. 18, 08 2022.

[4] G. Oriolo, *Wheeled Robots*. London: Springer London, 2020, pp. 1–8.

[5] X. Gao, L. Yan, and C. Gerada, "Modeling and analysis in trajectory tracking control for wheeled mobile robots with wheel skidding and slipping: Disturbance rejection perspective," *Actuators*, vol. 10, p. 222, 09 2021.

[6] J. Minguez, F. Lamiraux, and J.-P. Laumond, *Motion Planning and Obstacle Avoidance*. Springer, 01 2016, pp. 827–852.

[7] J. Li, J. Sun, and G. Chen, "A multi-switching tracking control scheme for autonomous mobile robot in unknown obstacle environments," *Electronics*, vol. 9, no. 1, pp. 1–14, 2020.

[8] T. Yang, N. Sun, and Y. Fang, "Adaptive fuzzy control for a class of mimo underactuated systems with plant uncertainties and actuator deadzones: Design and experiments," *IEEE Transactions on Cybernetics*, vol. 52, no. 8, pp. 8213–8226, 2022.

[9] B. Siciliano and O. Khatib, *Springer Handbook of Robotics*, 2nd ed. Springer Publishing Company, Incorporated, 2016.

[10] T. Dierks and S. Jagannathan, "Asymptotic adaptive neural network tracking control of nonholonomic mobile robot formations," *Journal of Intelligent and Robotic Systems*, vol. 56, no. 1, pp. 153–176, 2009.

[11] N. A. Martins and D. W. Bertol, *Wheeled Mobile Robot Control: Theory, Simulation, and Experimentation*, 1st ed. Springer Nature Switzerland AG, 2022.

[12] Y. Liu and R. Bucknall, "A survey of formation control and motion planning of multiple unmanned vehicles," *Robotica*, vol. 36, no. 7, pp. 1019–1047, 03 2018.

[13] N. Hassan and A. Saleem, "Neural network-based adaptive controller for trajectory tracking of wheeled mobile robots," *IEEE Access*, vol. 10, pp. 13 582–13 597, 2022.

[14] W. Liu, X. Wang, and S. Li, "Formation control for leader-follower wheeled mobile robots based on embedded control technique," *IEEE Transactions on Control Systems Technology*, vol. 31, no. 1, pp. 265–280, 2023.

[15] K. Sun, Z. Xu, S. Li, X. Li, and X. Zhou, "Robust trajectory tracking control of wheeled mobile robots and comparison with existing methods," in *2022 41st Chinese Control Conference (CCC)*, 2022, pp. 2749–2754.

[16] V. Utkin, A. Poznyak, Y. Orlov, and A. Polyakov, *Road Map for Sliding Mode Control Design*, 1st ed. Springer Cham, 2020.

[17] A. Mehta and B. Bandyopadhyay, *Emerging Trends in Sliding Mode Control - Theory and Application*. Springer, 09 2020.

[18] V. Utkin, J. Guldner, and J. Shi, *Sliding Mode Control in Electro-Mechanical Systems*, 2nd ed. CRC Press, 01 2017.

[19] P.-Z. Lin, C. Hsu, T.-T. Lee, and C.-H. Wang, "Robust fuzzy-neural sliding-mode controller design via network structure adaptation," *Control Theory & Applications, IET*, vol. 2, pp. 1054 – 1065, 01 2009.

[20] X. Yu, F. Yang, Y. Huang, and H. Nan, "Fuzzy immune sliding mode control based hydro turbine governor," in *Third International Conference on Natural Computation (ICNC 2007)*, vol. 1, 2007, pp. 171–176.

[21] ——, "Adaptive fuzzy immune sliding mode control for a class of uncertain nonlinear systems," in *Fourth International Conference on Fuzzy Systems and Knowledge Discovery (FSKD 2007)*, vol. 2, 2007, pp. 546–550.

[22] X. Yu, J. Tian, Y. Huang, and H. Nan, "Adaptive double immune sliding mode control for a class of uncertain nonlinear systems," in *2008 IEEE International Conference on Fuzzy Systems (IEEE World Congress on Computational Intelligence)*, 2008, pp. 1199–1203.

[23] W. Lin, H.-K. Chiang, and Y. Chung, "The speed control of immune-fuzzy sliding mode controller for a synchronous reluctance motor," *Applied Mechanics and Materials*, vol. 300-301, pp. 1490–1493, 02 2013.

[24] C. Sun, G. Guofang, and H. Yang, "Sliding mode control with

adaptive fuzzy immune feedback reaching law," *International Journal of Control, Automation and Systems*, vol. 18, 08 2019.
[25] Y. Zheng, J. Zheng, K. Shao, H. Zhao, Z. Man, and Z. Sun, "Adaptive fuzzy sliding mode control of uncertain nonholonomic wheeled mobile robot with external disturbance and actuator saturation," *Information Sciences*, vol. 663, p. 120303, 2024.
[26] B. Chai, K. Zhang, M. Tan, and J. Wang, "An optimal robust trajectory tracking control strategy for the wheeled mobile robot," *International Journal of Control, Automation and Systems*, vol. 22, pp. 1050—-1065, 01 2024.
[27] M. Sani, B. Robu, and A. Hably, "Dynamic obstacles avoidance using nonlinear model predictive control," in *IECON 2021 – 47th Annual Conference of the IEEE Industrial Electronics Society*, Oct 2021, pp. 1–6.
[28] Y. Wang, X. Li, J. Zhang, S. Li, Z. Xu, and X. Zhou, "Review of wheeled mobile robot collision avoidance under unknown environment," *Science Progress*, vol. 104, no. 3, p. 00368504211037771, 2021.
[29] M. Mosayebi and P. Mallahi Kolahi, "Time optimal trajectory generation with obstacle avoidance by using optimal control theory for a wheeled mobile robot," *Gazi University Journal of Science*, vol. 36, no. 1, p. 430–439, 2023.
[30] J. Zhang, D. Wei, R. Gao, and Z. Xia, "A trajectory tracking and obstacle avoidance approach for nonholonomic mobile robots based on model predictive control," in *2020 IEEE 16th International Conference on Control & Automation (ICCA)*, 2020, pp. 1038–1043.
[31] H.-Y. Lin, S.-H. Tsai, and K.-Y. Chen, "Design and implementation of the trajectory tracking and dynamic obstacle avoidance of wheeled mobile robot based on t-s fuzzy model," *International Journal of Fuzzy Systems*, vol. 25, no. 6, pp. 2423–2438, 2023.
[32] A. Rosales, G. Scaglia, V. Mut, and F. Sciascio, "Trajectory tracking of mobile robots in dynamic environments - a linear algebra approach," *Robotica*, vol. 27, no. 7, pp. 981–997, 12 2009.
[33] S. Mastellone, D. Stipanovic, C. Graunke, K. Intlekofer, and M. Spong, "Formation control and collision avoidance for multi-agent non-holonomic systems: Theory and experiments," *I. J. Robotic Res.*, vol. 27, pp. 107–126, 01 2008.
[34] M. Begnini, D. W. Bertol, and N. A. Martins, "A robust adaptive fuzzy variable structure tracking control for the wheeled mobile robot: Simulation and experimental results," *Control Engineering Practice*, vol. 64, pp. 27–43, 2017.
[35] E. Elyoussef, N. Martins, D. Bertol, E. Pieri, and U. Moreno, "Simulation results and practical implementation of a pd-super-twisting second order sliding mode tracking control for a differential wheeled mobile robot," *International Journal of Computer Applications in Technology*, vol. 63, p. 213, 01 2020.
[36] W. J. N. Goto and N. A. Martins, "Leader-follower formation tracking for differential-drive wheeled mobile robots with uncertainties and disturbances based on immune fuzzy quasi-sliding mode control," *Journal of the Brazilian Society of Mechanical Sciences and Engineering*, vol. 46, no. 2, p. 91, Jan 2024. [Online]. Available: https://doi.org/10.1007/s40430-023-04650-8
[37] W. J. N. Goto, D. W. Bertol, and N. A. Martins, "Formation and trajectory tracking of mobile robots with uncertainties and disturbances using an adaptive immune fuzzy quasi-sliding mode control," *Journal of Control, Automation and Electrical Systems*, vol. 35, no. 3, pp. 440–460, Jun 2024. [Online]. Available: https://doi.org/10.1007/s40313-024-01089-7
[38] D. Dasgupta, "Advances in artificial immune systems," *IEEE Computational Intelligence Magazine*, vol. 1, no. 4, pp. 40–49, 2006.
[39] A. Dai, X. Zhou, and X. Liu, "Design and simulation of a genetically optimized fuzzy immune pid controller for a novel grain dryer," *IEEE Access*, vol. 5, pp. 14 981–14 990, 2017.
[40] R. Bouchebbat and S. Gherbi, "Design and application of fuzzy immune pid adaptive control based on particle swarm optimization in thermal power plants," in *2017 6th International Conference on Systems and Control (ICSC)*, 2017, pp. 33–38.
[41] P. Chu, Y. Yu, D. Dong, H. Lin, and J. Yuan, "Nsga-ii-based parameter tuning method and gm(1,1)-based development of fuzzy immune pid controller for automatic train operation system," *Mathematical Problems in Engineering*, vol. 2020, pp. 1–20, 2020.
[42] C.-H. Wang and K. Hor, "From fuzzy center average defuzzifier (cad) to fuzzy lookup table controller (fltc) with an efficient heaviside search algorithm (hsa)," *Neural Computing and Applications*, vol. 31, no. 9, pp. 5135–5145, 2019.
[43] H. Suwoyo, Y. Tian, and M. Hajar, "Enhancing the performance of the wall-following robot based on flc-ga," *SINERGI*, vol. 24, p. 141, 04 2020.
[44] M. W. Spong, S. Hutchinson, and M. Vidyasagar, *Robot Modeling and Control*, 2nd ed. John Wiley & Sons, Inc., 2020.
[45] A. Benzerrouk, L. Adouane, and P. Martinet, "Stable navigation in formation for a multi-robot system based on a constrained virtual structure," *Robotics and Autonomous Systems*, vol. 62, no. 12, pp. 1806–1815, 2014.
[46] M. Mancini, N. Bloise, E. Capello, and E. Punta, "Sliding mode control techniques and artificial potential field for dynamic collision avoidance in rendezvous maneuvers," *IEEE Control Systems Letters*, vol. 4, no. 2, pp. 313–318, 2020.
[47] M. Gu and Y. Huang, "Dynamic obstacle avoidance of mobile robot based on adaptive velocity obstacle," in *2021 36th Youth Academic Annual Conference of Chinese Association of Automation (YAC)*, 2021, pp. 776–781.
[48] A. Ferrara and M. Rubagotti, "A dynamic obstacle avoidance strategy for a mobile robot based on sliding mode control," in *2009 IEEE Control Applications, (CCA) & Intelligent Control, (ISIC)*, 2009, pp. 1535–1540.
[49] A. Nikranjbar, M. Haidari, and A. A. Atai, "Adaptive sliding mode tracking control of mobile robot in dynamic environment using artificial potential fields," *Journal of Computer and Robotics*, vol. 11, no. 1, pp. 1–14, 2018.
[50] A. Sadollah, *Introductory Chapter: Which Membership Function is Appropriate in Fuzzy System?* Rijeka: IntechOpen, 2018, ch. 1.
[51] F. Freire, N. Martins, and F. Splendor, "A simple optimization method for tuning the gains of pid controllers for the autopilot of cessna 182 aircraft using model-in-the-loop platform," *Journal of Control, Automation and Electrical Systems*, vol. 29, no. 4, pp. 441–450, 2018.
[52] K. Erbatur and B. Calli, "Fuzzy boundary layer tuning for sliding mode systems as applied to the control of a direct drive robot," *Soft Computing*, vol. 13, pp. 1099–1111, 06 2009.